Optimal Control Strategies for COVID-19 Epidemic Management: A Mathematical Modeling Approach Using the SEIQR Framework

Ramesh Ramalingam[1], Arul Joseph Gnanaprakasam[2] and Salah Boulaaras[3,*]

[1] Department of Mathematics, Faculty of Engineering and Technology, SRM Institute of Science and Technology, Ramapuram, Chennai, 600089, Tamil Nadu, India

[2] Department of Mathematics, College of Engineering and Technology, SRM Institute of Science and Technology, SRM Nagar, Kattankulathur, Kanchipuram, Chennai, 603203, Tamil Nadu, India

[2] Department of Mathematics, College of Science, Qassim University, Buraydah, 51452, Saudi Arabia

INFORMATION

Keywords:
Lyapunov functions
global stability
Pontryagin's maximum principle
optimal control
COVID-19 pandemic
mathematical models

DOI: 10.23967/j.rimni.2025.10.63464

SCIPEDIA Revista Internacional de Métodos Numéricos para Cálculo y Diseño en Ingeniería

Revista Internacional Métodos numéricos para cálculo y diseño en ingeniería RIMNI CIMNE

Optimal Control Strategies for COVID-19 Epidemic Management: A Mathematical Modeling Approach Using the SEIQR Framework

Ramesh Ramalingam[1], Arul Joseph Gnanaprakasam[2] and Salah Boulaaras[3,*]

[1]Department of Mathematics, Faculty of Engineering and Technology, SRM Institute of Science and Technology, Ramapuram, Chennai, 600089, Tamil Nadu, India

[2]Department of Mathematics, College of Engineering and Technology, SRM Institute of Science and Technology, SRM Nagar, Kattankulathur, Kanchipuram, Chennai, 603203, Tamil Nadu, India

[3]Department of Mathematics, College of Science, Qassim University, Buraydah, 51452, Saudi Arabia

ABSTRACT

The COVID-19 pandemic has necessitated the development of robust mathematical models to understand and mitigate its impact. This study presents a compartmental model for the Indian pandemic COVID-19 dynamics, incorporating key compartments such as susceptible, exposed, infected, quarantined, and recovered populations. The positivity and boundedness of solutions are rigorously analyzed to ensure that the model remains biologically meaningful over time. A detailed exploration of the basic reproduction number R_0 is conducted using the next-generation matrix approach, identifying it as a pivotal threshold parameter dictating disease dynamics. The equilibria of the system, including the Disease-Free Equilibrium (DFE) and the Endemic Equilibrium (EE), are derived and analyzed for their stability properties. The local stability of the DFE is established for $R_0 < 1$, while conditions for the existence and stability of the EE are explored for $R_0 > 1$. Additionally, the study employs Lyapunov functions to assess the global stability of equilibria, ensuring the robustness of the proposed model under varying initial conditions. The Pontryagin's Maximum Principle is utilized to derive optimal control strategies, focusing on minimizing the number of infections and optimizing interventions such as vaccination, treatment, and quarantine measures like wearing a face mask and hand washing. Numerical simulations validate the theoretical findings, providing critical insights into the effectiveness of various control measures. This comprehensive framework contributes to the mathematical understanding of COVID-19 dynamics and offers valuable guidance for public health decision-making.

OPEN ACCESS

Received: 15/01/2025

Accepted: 11/03/2025

Published: 07/04/2025

DOI
10.23967/j.rimni.2025.10.63464

Keywords:
Lyapunov functions
global stability
Pontryagin's maximum principle
optimal control
COVID-19 pandemic
mathematical models

*Correspondence: Salah Boulaaras (s.boularas@qu.edu.sa). This is an article distributed under the terms of the Creative Commons BY-NC-SA license

1 Introduction

The study of infectious diseases has evolved significantly since Bernoulli's pioneering work on smallpox mortality in 1760 [1]. Kermack and McKendrick's foundational epidemic model in 1927 laid the groundwork for modern mathematical epidemiology [2]. Subsequent advancements, such as Krener's maximal principle [3] and Guckenheimer and Holmes' exploration of nonlinear dynamics [4], further enriched the theoretical framework. The concept of the basic reproduction number (R_0) was rigorously defined by Diekmann et al. in 1990, providing a critical metric for disease spread in heterogeneous populations [5].

Coronavirus Disease 2019 (COVID-19) is a respiratory illness caused by the Severe Acute Respiratory Syndrome Coronavirus 2 (SARS-CoV-2) [6]. First identified in Wuhan, China, in late 2019, the virus rapidly propagated worldwide, leading the World Health Organization (WHO) to declare it a pandemic on 11 March 2020. As of 2023 [7], the global impact has been profound, with millions of infections and significant mortality [8].

Transmission primarily occurs through respiratory droplets emitted during coughing, sneezing, or talking. Contact with contaminated surfaces followed by touching the face can also facilitate infection [9]. The virus's zoonotic origins are under investigation, with studies suggesting a likely bat origin, potentially involving intermediate hosts [10].

SARS-CoV-2 exhibits varying survival times on different surfaces, persisting longer on non-porous materials like glass, metal, and plastics [11]. The incubation period ranges from 2 to 14 days, with common symptoms including fever, fatigue, dry cough, and dyspnea [12]. Preventive measures such as hand hygiene, mask-wearing, and social distancing are crucial in mitigating transmission.

In response to the pandemic's severity, countries worldwide implemented measures including lockdowns, travel restrictions, and the closure of public spaces. While effective in controlling viral spread, these interventions had significant socio-economic repercussions. The International Monetary Fund (IMF) projected a global economic contraction of 3% in 2020, highlighting the pandemic's economic toll [13].

India, with its vast and densely populated regions, faced unique challenges. Since the first reported case in January 2020, the country has experienced multiple waves of infections. As of 2022, India reported over 43 million confirmed cases and more than 525,000 fatalities [14]. The second wave, in particular, overwhelmed the healthcare system, leading to shortages of medical supplies and hospital beds.

Factors contributing to the severity of India's second wave included the emergence of more transmissible variants and lapses in adherence to public health measures [15]. Delays in vaccine rollout further exacerbated the situation, underscoring the need for timely and effective vaccination strategies [16].

The literature is abundant of similar study as follows: Optimal control theory, as applied to biological systems by Lenhart et al. [17], has been instrumental in designing intervention strategies. Buonomo et al. extended this to vaccination models, emphasizing the role of information dissemination [18]. Recent studies, such as Li et al.'s analysis of hemorrhagic fever in China [19] and Kar et al.'s investigation of media impact on epidemic dynamics [20], highlight the integration of real-world factors into mathematical models.

The COVID-19 pandemic has spurred extensive research, including early transmission studies in Li et al. [21] and clinical characterizations of the disease [22]. Stability analysis using Lyapunov functions has provided insights into disease dynamics, while real-world data calibration, such as

Ethiopian COVID-19 cases from early 2022, has enhanced model accuracy. Global sensitivity analysis has further validated model robustness [23]. Non-pharmaceutical interventions (NPIs) have been critically analyzed for their effectiveness in mitigating the pandemic [24], and optimal control strategies combining vaccination, public health education, and treatment have proven most cost-effective.

India's experience with COVID-19, particularly the second wave, has been extensively documented [25]. Vaccination efforts, while ambitious, face significant challenges [26]. Socio-economic implications of the pandemic have been globally significant, as highlighted by Nicola et al. and the IMF [27].

This study aims to develop a mathematical model tailored to India's COVID-19 dynamics, incorporating compartments for susceptible, exposed, infected, quarantined, and recovered individuals. By analyzing the model's equilibria and stability, we seek to provide insights into the disease's progression and evaluate the impact of various control strategies, including preventive measures, medical interventions, and efforts to prevent reinfection among recovered individuals. Such a model can inform public health policies and optimize resource allocation in the ongoing battle against COVID-19.

2 Model Formulation

In this section, we will utilize a mathematical model to describe the entire population at time t, denoted as $Y(t)$. The total population is divided into five distinct categories: individuals who are susceptible ($S(t)$), those who have been exposed ($E(t)$), individuals infected with COVID-19 ($I(t)$), individuals who have been quarantined ($Q(t)$), and individuals who have recovered from COVID-19 ($R(t)$) [11].

We enhance the model by incorporating healthcare awareness and the possibility of individuals who have been quarantined ($Q(t)$) and tested negative for COVID-19 to return to the susceptible category ($S(t)$). Individuals in high-risk areas or in contact with confirmed COVID-19 cases are placed in the restricted division. These individuals are detained during the outbreak phase, and their bodies undergo virus infection screenings [11]. Individuals who receive a negative test result are placed back into the susceptible category ($S(t)$), whereas those who test positive are moved into the infectious quarantine category ($Q(t)$). Those who refuse isolation but still test positive are allocated to the infectious non-hospitalized compartment ($I(t)$), where they either recuperate due to their robust immunity or are shifted to the hospitalized/isolated infectious compartment [11]. The proposed model with the assumptions is as follows:

- The recruitment rate (A) is considered constant, assuming a steady inflow of individuals into the susceptible population through birth or immigration.
- The disease spread rate (β) accounts for interaction between susceptible individuals and infectious individuals. It is assumed that efforts like awareness campaigns and social distancing (v_1) effectively reduce contact rates.
- Exposed individuals transition to the infectious stage at a rate ϵ. This rate is influenced by the incubation period of COVID-19 and is assumed to be consistent across the population.
- Isolation measures (v_2) are assumed to effectively remove a portion of exposed or infectious individuals from the transmission cycle, reducing the active spread of the disease.
- Health awareness campaigns (v_1) are assumed to create widespread compliance with preventive measures like mask-wearing and physical distancing.

- Individuals in quarantine (Q) who test negative for COVID-19 are assumed to return to the susceptible population (S), reflecting successful containment of non-infected individuals.
- Individuals in high-risk zones or with direct exposure to confirmed cases are screened for infection and categorized appropriately into S, E, I, or Q.
- Handwashing and hygiene campaigns (v_3) are assumed to lower the risk of reinfection or secondary transmission within households and communities.
- Recovery rates (α_1 and α_2) are influenced by the availability of medical facilities, treatment protocols, and public health interventions.
- Natural death rate (γ) is constant, assuming demographic stability over the model's timeframe.
- The population is assumed to be homogeneously mixed, meaning every individual has an equal probability of interacting with others.
- Vaccination effects are not explicitly included, focusing primarily on non-pharmaceutical interventions.
- The effectiveness of awareness campaigns, isolation, and hygiene measures is assumed to be proportional to the respective control efforts (v_1, v_2, v_3).
- Individuals in the infectious non-hospitalized category (I) are assumed to either recover or progress to the hospitalized/isolated compartment based on their immunity and healthcare access.
- Natural death rate (γ) is constant, and COVID-19-induced mortality is not explicitly modeled, as the focus is on non-pharmaceutical interventions.

$$Y(t) = S(t) + E(t) + Q(t) + I(t) + R(t)$$

The presented mathematical model serves as a compartmental framework designed to capture the dynamics of COVID-19 transmission and control strategies. The population is categorized into distinct compartments: Susceptible (S), Exposed (E), Infectious (I), Quarantined (Q), and Recovered (R). Each compartment represents a specific stage in the progression of the disease, and the transitions between these groups are described using a system of ordinary differential equations. These equations account for the essential processes that govern disease transmission, exposure, infection, isolation, and recovery, offering a structured approach to analyze the impact of various intervention measures on controlling the spread of the virus [11].

The dynamics of the model are described by the following system of differential equations:

$$\begin{aligned}
\frac{dS}{dt} &= A - \beta SI - \gamma S \\
\frac{dE}{dt} &= \beta SI - (\gamma + \theta_2 + \epsilon)E \\
\frac{dI}{dt} &= \epsilon E - (\gamma + \theta_1 + \alpha_1)I \\
\frac{dQ}{dt} &= \theta_1 I + \theta_2 E - (\alpha_2 + \gamma)Q \\
\frac{dR}{dt} &= \alpha_1 I + \alpha_2 Q - \gamma R
\end{aligned} \tag{1}$$

The initial states of the system are:
$S(0) > 0, E(0) \geq 0, I(0) \geq 0, Q(0) \geq 0, R(0) \geq 0$

This model is based on several real-life and theoretical assumptions. First, it assumes homogeneous mixing within the population, meaning that every individual has an equal chance of coming into contact with an infectious individual. It also assumes that quarantined individuals do not contribute to the transmission of the disease, aligning with isolation protocols [11]. The recovery rates α_1 and α_2 are assumed to depend on the availability of medical resources and the effectiveness of treatment. The disease-induced mortality is not explicitly included, with the model focusing on natural mortality rates.

Furthermore, the recruitment rate (A) represents births or migration, ensuring a continuous inflow into the population. It is assumed that the parameters governing the model, such as $\beta, \epsilon, \theta_1$, and θ_2, are constant throughout analysis, although in reality, these may vary due to interventions like vaccination or changes in public behavior [11]. This simplification aids in mathematical tractability but may limit the model's ability to capture dynamic changes in disease transmission.

This framework provides a foundation for exploring various control strategies, such as increasing quarantine efficiency or enhancing public health awareness to reduce β. By calibrating the model with real-world data, it can be adapted to predict the outcomes of different intervention measures, thereby assisting policymakers in designing effective responses to the pandemic. The model equations are derived from the schematic representation depicted in Fig. 1 [11].

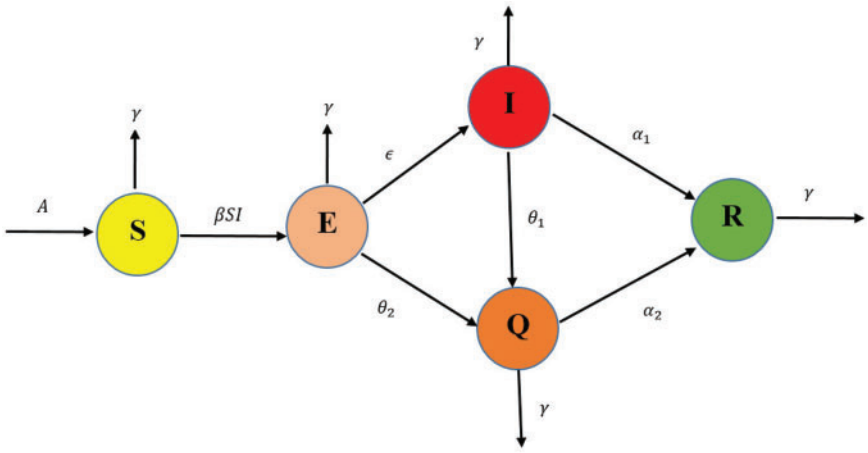

Figure 1: Compartmental diagram of SEQIR model for Indian COVID-19 pandemic

Table 1 and Fig. 1 provide a detailed description of the parameters used in the epidemiological model. Each parameter represents a specific aspect of the population dynamics, such as recruitment, disease transmission, progression, quarantine, recovery, and natural death rates. These parameters collectively define the transitions between different compartments of the model, offering a comprehensive framework to analyze disease spread and control mechanisms.

Table 1: Descriptions of parameters in the model

Parameter	Description
A	Refers to the recruitment rate, representing the number of individuals entering the susceptible population, such as through births or migration.
β	Indicates the transmission rate of the disease from susceptible individuals (S) to the exposed category (E).
ϵ	Represents the progression rate at which exposed individuals (E) become infectious (I).
θ_1	Denotes the rate at which infected individuals (I) are quarantined (Q) to limit disease transmission.
θ_2	Specifies the rate at which exposed individuals (E) are quarantined (Q) to prevent further spread of the infection.
α_1	Defines the recovery rate of infected individuals (I) who recover and move to the recovered category (R).
α_2	Represents the recovery rate of quarantined individuals (Q) transitioning to the recovered category (R).
γ	Accounts for the natural death rate, which is unrelated to the disease under study.

3 Positivity and Boundedness Analysis

3.1 Positivity Analysis

Theorem 3.1. ***Non-Negativity of Solutions*** *Let $S(t)$, $E(t)$, $I(t)$, $Q(t)$, and $R(t)$ denote the solutions of the system described in (1), subject to the initial conditions $S(0) > 0$, $E(0) \geq 0$, $I(0) \geq 0$, $Q(0) \geq 0$, and $R(0) \geq 0$. Then, for all $t \geq 0$, these solutions remain non-negative, satisfying the following* [17,18]:

$$S(t) > 0, \quad E(t) \geq 0, \quad I(t) \geq 0, \quad Q(t) \geq 0, \quad R(t) \geq 0$$

Proof: To ensure the positivity of the solutions $S(t)$, $E(t)$, $I(t)$, $Q(t)$, and $R(t)$, we analyze each equation in the system. Starting with $S(t)$, the rate of change $\frac{dS}{dt} = A - \beta SI - \gamma S$ indicates that $A > 0$ is a positive inflow term, while $-\beta SI$ and $-\gamma S$ are non-positive. Thus, as long as $S(0) > 0$, $S(t)$ remains non-negative for $t \geq 0$. Similarly, for $E(t)$, the equation $\frac{dE}{dt} = \beta SI - (\gamma + \theta_2 + \epsilon)E$ ensures non-negativity since $\beta SI \geq 0$ and the second term $-(\gamma + \theta_2 + \epsilon)E$ acts as a damping term for$E$. Provided $E(0) \geq 0$, it follows that $E(t) \geq 0$. The same reasoning applies to $I(t)$, where $\frac{dI}{dt} = \epsilon E - (\gamma + \theta_1 + \alpha_1)I$ guarantees non-negative solutions, as $\epsilon E \geq 0$ and the second term ensures $I(t)$ does not decrease below zero if $I(0) \geq 0$. For $Q(t)$, the equation $\frac{dQ}{dt} = \theta_1 I + \theta_2 E - (\alpha_2 + \gamma)Q$ ensures positivity because the first two terms are non-negative, and the damping term prevents $Q(t)$ from becoming negative given $Q(0) \geq 0$. Finally, $R(t)$, governed by $\frac{dR}{dt} = \alpha_1 I + \alpha_2 Q - \gamma R$, remains non-negative since both $\alpha_1 I$ and $\alpha_2 Q$ are positive terms, while $-\gamma R$ does not drive $R(t)$ below zero. Therefore, under

non-negative initial conditions and parameters, the solutions of the system remain non-negative for all $t \geq 0$ [11]. □

3.2 Boundedness of Solutions

Theorem 3.2. ***Boundedness of Solutions*** *The solutions $S(t)$, $E(t)$, $I(t)$, $Q(t)$, and $R(t)$ are uniformly bounded for all $t \geq 0$. In particular, there exists a positive constantN such that:*

$$S(t) + E(t) + I(t) + Q(t) + R(t) \leq N \quad \text{for all } t \geq 0$$

Proof: The analysis of boundedness demonstrates that the solutions of the system remain finite and do not grow without limit as time progresses. This ensures that the variables are confined within biologically or physically meaningful ranges. Formally, our goal is to show that: Let $Y(t) = S(t) + E(t) + Q(t) + I(t) + R(t)$

then

$$\frac{dY}{dt} = \frac{dS}{dt} + \frac{dE}{dt} + \frac{dI}{dt} + \frac{dQ}{dt} + \frac{dR}{dt}$$

$$\frac{dY}{dt} = A - \gamma Y$$

$$\frac{dY}{dt} + \gamma Y \leq A$$

The solution of the proposed model remains bounded. Integrating the above inequality using the theorem of differential equations by Birkhoff and Rota [17,18], we obtain:

$$Y \leq \frac{A}{\gamma}[1 - e^{-\gamma t}] + Y_0 e^{-\gamma t} \tag{2}$$

now for $\boldsymbol{t} \to \infty$

$$0 < Y(S, E, I, Q, R) \leq \frac{A}{\gamma}$$

Hence, all the solutions of the system of nonlinear Eq. (1) that commence in R_+^5 are restricted to the region [17,18]. □

4 Basic Reproduction Number R_0

The basic reproduction number R_0 represents the average number of secondary infections produced by a single infected individual in a population consisting entirely of susceptible individuals. This value is computed using the next-generation matrix approach, where $F(P)$ represents the vector for new infections and $V(P)$ represents the vector for transmission and transition into disease compartments. The basic reproduction number is derived from the next-generation matrix methodology, utilizing $F(P)$ to denote the vector for new infections and $V(P)$ to denote the vector for transmission and transition into disease compartments [28].

$$\begin{aligned}
\frac{dE}{dt} &= \beta SI - [\gamma + \epsilon + \theta_2]E \\
\frac{dI}{dt} &= \epsilon E - [\gamma + \theta_1 + \alpha_1]I \\
\frac{dQ}{dt} &= \theta_1 I + \theta_2 E - [\gamma + \alpha_2]Q
\end{aligned} \tag{3}$$

We can write the above system as:

$$\frac{dp}{dt} = F(P) - V(P)$$

$$P = \begin{pmatrix} E \\ I \\ Q \end{pmatrix}, F(P) = \begin{pmatrix} \beta SI \\ 0 \\ 0 \end{pmatrix}, V(P) = \begin{pmatrix} (\gamma + \epsilon + \theta_2)E \\ (\gamma + \theta_1 + \alpha_1)I - \epsilon E \\ (\gamma + \alpha_2)Q - \theta_1 I - \theta_2 E \end{pmatrix}$$

The inclusion of $Q(t)$ in the system is crucial because quarantined individuals may still affect the disease dynamics by preventing transmission through isolation while also contributing indirectly to reducing the susceptible population's exposure to infected individuals.

From Eq. (1), a disease-free equilibrium equation that is not linear, denoted as $E_0\left(\frac{A}{\gamma}, 0, 0, 0, 0\right)$, the Jacobian matrices of $F(P)$ and $V(P)$ at the disease-free equilibrium are given by:

$$F(P) = J\left(\frac{F(P)}{E_0}\right) = \begin{pmatrix} 0 & \beta S^0 & 0 \\ 0 & 0 & 0 \\ 0 & 0 & 0 \end{pmatrix}$$

$$V(P) = J\left(\frac{V(P)}{E_0}\right) = \begin{pmatrix} \gamma + \theta_2 + \epsilon & 0 & 0 \\ -\epsilon & \gamma + \theta_1 + \alpha_1 & 0 \\ -\theta_2 & -\theta_1 & \gamma + \alpha_2 \end{pmatrix}$$

Then

$$V^{-1} = \begin{pmatrix} \frac{1}{\gamma + \theta_2 + \epsilon} & 0 & 0 \\ \frac{\epsilon}{(\gamma + \theta_2 + \epsilon)(\gamma + \theta_1 + \alpha_1)} & \frac{1}{\gamma + \theta_1 + \alpha_1} & 0 \\ \frac{\epsilon\theta_1 + \theta_2(\gamma + \theta_1 + \alpha_1)}{(\gamma + \theta_2 + \epsilon)(\gamma + \theta_1 + \alpha_1)(\gamma + \alpha_2)} & \frac{\theta_1}{(\gamma + \theta_1 + \alpha_1)(\gamma + \alpha_2)} & \frac{1}{\gamma + \alpha_2} \end{pmatrix}$$

The spectral radius of the matrix, also referred to as the basic reproduction number R_0, represented as $F(P)V^{-1}$, is denoted in the present model as:

$$F(P)V^{-1} = \begin{pmatrix} 0 & \beta S_0 & 0 \\ 0 & 0 & 0 \\ 0 & 0 & 0 \end{pmatrix} \begin{pmatrix} \frac{1}{\gamma+\theta_2+\epsilon} & 0 & 0 \\ \frac{\epsilon}{(\gamma+\theta_2+\epsilon)(\gamma+\theta_1+\alpha_1)} & \frac{1}{\gamma+\theta_1+\alpha_1} & 0 \\ \frac{\epsilon\theta_1+\theta_2(\gamma+\theta_1+\alpha_1)}{(\gamma+\theta_2+\epsilon)(\gamma+\theta_1+\alpha_1)(\gamma+\alpha_2)} & \frac{\theta_1}{(\gamma+\theta_1+\alpha_1)(\gamma+\alpha_2)} & \frac{1}{\gamma+\alpha_2} \end{pmatrix}$$

The initial illness transmission number R_0 of the matrix $F(P)V^{-1}$ is given by:

$$R_0 = F(P)V^{-1} = \frac{\beta\epsilon S_0}{(\gamma+\theta_2+\epsilon)(\gamma+\theta_1+\alpha_1)} = \frac{A\beta\epsilon}{\gamma(\gamma+\theta_2+\epsilon)(\gamma+\theta_1+\alpha_1)} \tag{4}$$

Fig. 2 demonstrates the dependence of R_0 on the transmission rate (β) and natural mortality rate (γ). R_0 increases with β, highlighting the role of contact rate in spreading disease, while higher γ suppresses R_0 by reducing susceptibility. The maximum R_0 is approximately 2.45.

Fig. 3 provides a contour plot of R_0 against β and γ, showing consistent patterns. Higher β increases R_0, whereas increasing γ reduces it, effectively capturing the interplay between these parameters in disease dynamics.

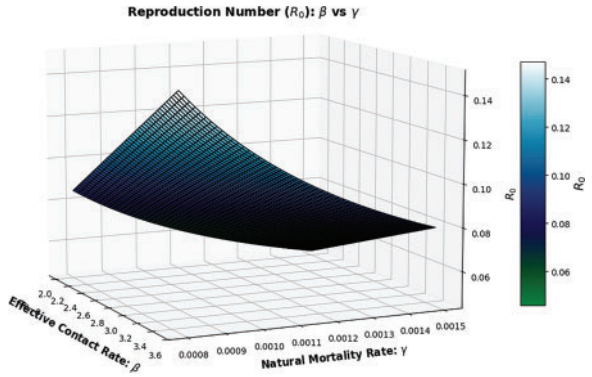

Figure 2: Surface plot on effect of disease transmission rate (β) and natural death rate (γ) on R_0

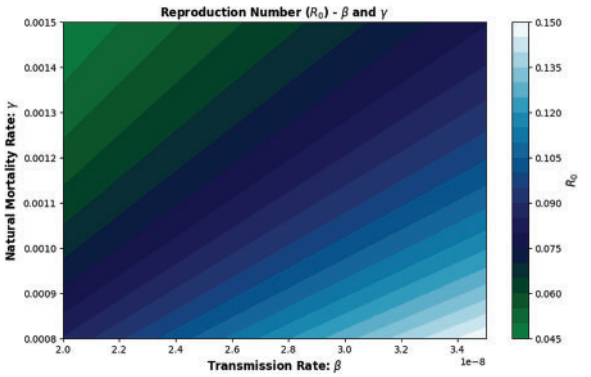

Figure 3: Contour plot on effect of disease transmission rate (β) and natural death rate (γ) on R_0

Fig. 4 shows R_0 as a function of β and the recovery rate (α_1). While R_0 decreases with higher α_1, a rise in β still drives it upward, emphasizing the dominant effect of contact rates. The maximum R_0 remains at 2.45.

Fig. 5 presents a contour plot for R_0 with β and α_1. It highlights the proportionality between β and R_0, while α_1 reduces R_0, confirming its mitigating impact on disease spread.

In Fig. 6, R_0 is analyzed with β and the quarantined recovery rate (α_2). Higher α_2 significantly reduces R_0, demonstrating the effectiveness of quarantine. The maximum R_0 here is the lowest, at approximately 1.49.

Fig. 7 shows a contour plot of R_0 with β and α_2. While β raises R_0, increasing α_2 results in a sharp decline, underlining quarantine measures as crucial in controlling transmission.

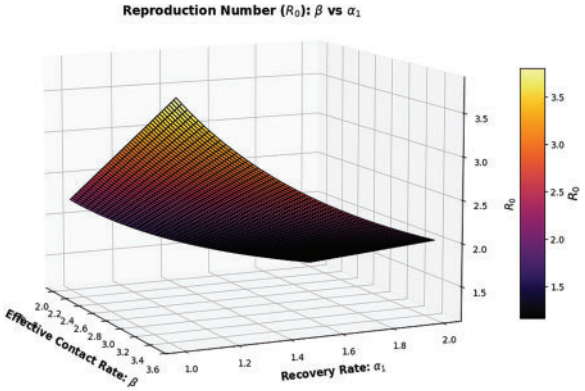

Figure 4: Surface plot on effect of disease transmission rate (β) and recovery rate of infected individuals (α_1) on R_0

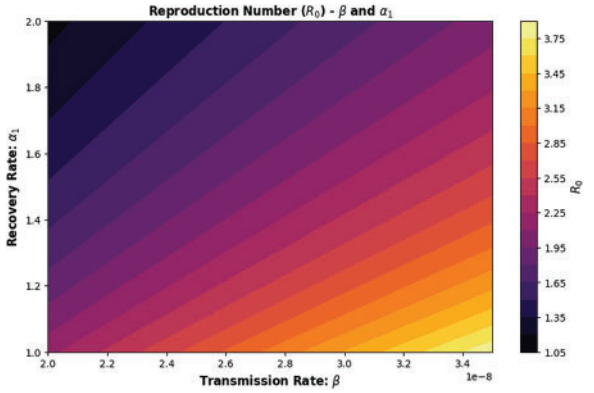

Figure 5: Contour plot on effect of disease transmission rate (β) and recovery rate of infected individuals (α_1) on R_0

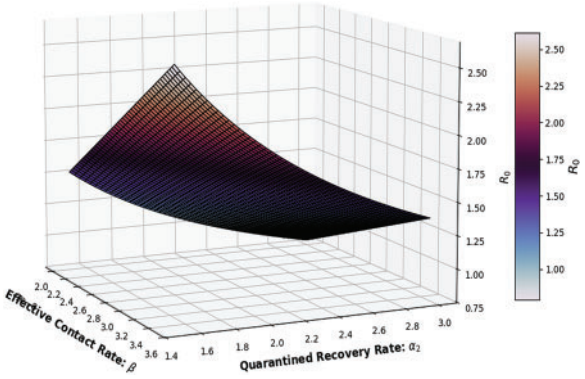

Figure 6: Surface plot on effect of disease transmission rate (β) and recovery rate of quarantined individuals (α_2) on R_0

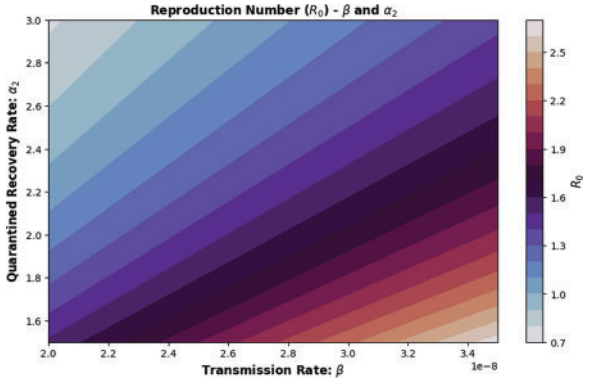

Figure 7: Contour plot on effect of disease transmission rate (β) and recovery rate of quarantined individuals (α_2) on R_0

The basic reproduction number, R_0, remains a vital metric in understanding disease spread. When $R_0 > 1$, it signals potential outbreaks, emphasizing its significance in epidemiological studies.

5 Equilibria Solution of Indian Pandemic COVID-19

The system exhibits two equilibrium states:

Disease-Free Equilibrium (DFE): Represented as E_0, this state is free of infections and is determined by the initial susceptible population S_0. The DFE is defined as:

$$E_0 = (S_0, 0, 0, 0, 0)$$

where $S_0 = \dfrac{A}{\gamma}$ and the basic reproduction number is:

$$R_0 = \frac{A\beta\epsilon}{\gamma(\gamma + \theta_2 + \epsilon)(\gamma + \theta_1 + \alpha_1)}$$

Endemic Equilibrium (EE): Denoted as $E_1 = (S^*, E^*, I^*, Q^*, R^*)$, this equilibrium represents a state where the infection persists in the population. At this point, all compartments (S, E, I, Q, and R) attain steady-state, nonzero values [29].

To determine these equilibria, the system of equations is solved by setting all derivatives to zero:

$$\frac{dS}{dt} = \frac{dE}{dt} = \frac{dI}{dt} = \frac{dQ}{dt} = \frac{dR}{dt} = 0$$

Solving this system yields the equilibrium points E_0 and E_1. The stability of these equilibria is analyzed using the Jacobian matrix and its eigenvalues [30].

In conclusion, the stability of the DFE ($R_0 < 1$) serves as a critical benchmark for controlling infectious diseases. Achieving and maintaining this stability through effective public health strategies is essential for eradicating the disease and preventing future outbreaks [11].

$$\begin{aligned}
S^* &= \frac{A}{\gamma} \cdot \frac{1}{R_0}, \\
E^* &= \frac{A\beta\epsilon}{\gamma(\gamma+\theta_2+\epsilon)(\gamma+\theta_1+\alpha_1)} \cdot \frac{R_0-1}{R_0}, \\
I^* &= \frac{A}{\beta} \cdot \frac{R_0-1}{R_0}, \\
Q^* &= \frac{\epsilon\theta_1 E^*}{(\gamma+\theta_1+\alpha_1)(\alpha_2+\gamma)} + \frac{\theta_2 E^*}{\alpha_2+\gamma}, \\
R^* &= \frac{\alpha_1 I^* + \alpha_2 Q^*}{\gamma}
\end{aligned} \tag{5}$$

6 Local Stability Analysis

Theorem 6.1. *The disease-free equilibrium E_0 of the system (1) is locally asymptotically stable if $R_0 \leq 1$.*

Proof: we examine the conditions under which the disease-free equilibrium (E_0) exists and its stability. The disease-free equilibrium is stable when the basic reproduction number $R_0 \leq 1$, and it becomes unstable when $R_0 > 1$. The Jacobian matrix of the system at the disease-free equilibrium E_0, which corresponds to $S = S_0$, $E = E_0$, $I = I_0$, $Q = Q_0$, and $R = R_0$, is given by:

$$J = \begin{bmatrix}
-\gamma & 0 & -\beta S_0 & 0 & 0 \\
0 & -(\gamma+\theta_2+\epsilon) & \beta S_0 & 0 & 0 \\
0 & \epsilon & -(\gamma+\theta_1+\alpha_1) & 0 & 0 \\
0 & \theta_2 & \theta_1 & -(\gamma+\alpha_2) & 0 \\
0 & 0 & \alpha_1 & \alpha_2 & -\gamma
\end{bmatrix}$$

The characteristic equation of this Jacobian matrix is given by:

$$|J - \tau I| = 0$$

which yields:

$$\begin{vmatrix} -\gamma-\tau & 0 & -\beta S_0 & 0 & 0 \\ 0 & -(\gamma+\theta_2+\epsilon)-\tau & \beta S_0 & 0 & 0 \\ 0 & \epsilon & -(\gamma+\theta_1+\alpha_1)-\tau & 0 & 0 \\ 0 & \theta_2 & \theta_1 & -(\gamma+\alpha_2)-\tau & 0 \\ 0 & 0 & \alpha_1 & \alpha_2 & -\gamma-\tau \end{vmatrix}$$

Expanding the determinant leads to the characteristic equation:

$$(\tau+\gamma)^2(\tau+\alpha_2+\gamma)\left(\tau^2+A_1\tau+A_1(1-R_0)\right)=0$$

where $A_1=(\gamma+\theta_1+\alpha_1)(\gamma+\theta_2+\epsilon)$.

From this, we can conclude the following:

1. When $R_0 \leq 1$, the disease-free equilibrium is locally asymptotically stable. The system exhibits infection-free stability, which indicates that the disease does not persist in the population.

2. When $R_0 > 1$, the disease-free equilibrium becomes unstable, and the system will transition to an endemic equilibrium where the disease persists in the population.

3. At $R_0 = 1$, a transcritical bifurcation occurs, indicating a shift in the stability of the equilibrium point. This transition marks the threshold for the disease's ability to spread within the population.

Thus, the stability analysis of the disease-free equilibrium is governed by the value of R_0. If $R_0 > 1$, the disease will persist, while if $R_0 \leq 1$, the disease will be eradicated from the population. This analysis is critical for understanding the dynamics of the disease and planning control strategies. □

Theorem 6.2. *The endemic equilibrium E_1 of the system (1) is locally asymptotically stable if $R_0 > 1$.*

Proof: We now examine the local asymptotic stability of the endemic equilibrium E_1 of the system. The endemic equilibrium E_1 is locally asymptotically stable when the basic reproduction number $R_0 \sim > \sim 1$. The Jacobian matrix of the system at the endemic equilibrium is given by [3]:

$$J(E_1)=\begin{bmatrix} -(\beta I^*+\gamma) & 0 & -\beta S^* & 0 & 0 \\ \beta I^* & -(\gamma+\theta_2+\epsilon) & \beta S^* & 0 & 0 \\ 0 & \epsilon & -(\gamma+\theta_1+\alpha_1) & 0 & 0 \\ 0 & \theta_2 & \theta_1 & -(\gamma+\alpha_2) & 0 \\ 0 & 0 & \alpha_1 & \alpha_2 & -\gamma \end{bmatrix}$$

To find the stability of the endemic equilibrium, we compute the determinant of $J-\tau I$, which is the characteristic equation of the system:

$$|J-\tau I|=\left|\begin{bmatrix} -(\beta I^*+\gamma)-\tau & 0 & -\beta S^* & 0 & 0 \\ \beta I^* & -(\gamma+\theta_2+\epsilon)-\tau & \beta S^* & 0 & 0 \\ 0 & \epsilon & -(\gamma+\theta_1+\alpha_1)-\tau & 0 & 0 \\ 0 & \theta_2 & \theta_1 & -(\gamma+\alpha_2)-\tau & 0 \\ 0 & 0 & \alpha_1 & \alpha_2 & -\gamma-\tau \end{bmatrix}\right|=0$$

This leads to the following characteristic equation:

$$(\tau+\gamma)^2(\tau+\alpha_2+\gamma)(\tau+(\gamma+R_0))(\tau+B_1)(\tau+B_2)(\gamma(1-R_0)-\beta(\tau C+R_0))=0$$

where,

$$B_1 = (\gamma + \theta_2 + \epsilon), \quad B_2 = (\gamma + \theta_1 + \alpha_1), \quad C = \frac{A\epsilon}{R_0}$$

Equilibrium Values: We substitute the equilibrium values for S^*, I^*, E^*, Q^*, R^*:

$$S^* = \frac{A}{\gamma} \cdot \frac{1}{R_0}, \quad I^* = \frac{A}{\beta} \cdot \frac{R_0 - 1}{R_0}$$

Substituting these into the Jacobian matrix and characteristic equation ensures the correctness of the expression for $J(x_{EE})$.

To analyze stability, we apply the Routh-Hurwitz criterion to the characteristic polynomial. For the characteristic equation:

$$P(\tau) = (\tau + \gamma)^2(\tau + \alpha_2 + \gamma)(\tau + (\gamma + R_0))(\tau + B_1)(\tau + B_2)(\gamma(1 - R_0) - \beta(\tau C + R_0))$$

From the characteristic equation, we observe that the first pair of roots are real and positive. The remaining roots form a quadratic polynomial, assuming all parameters are positive.

To confirm the local asymptotic stability of the endemic equilibrium, we apply the **Routh-Hurwitz criterion**. This criterion ensures that all the roots of the characteristic equation have negative real parts when $R_0 > 1$, which guarantees that the endemic equilibrium is locally asymptotically stable.

Thus, when $R_0 > 1$, the system transitions from the disease-free equilibrium to an endemic equilibrium, where the disease persists in the population. If $R_0 \leq 1$, the disease-free equilibrium remains stable, and the disease will eventually die out.

In summary, the endemic equilibrium E_1 is locally asymptotically stable when $R_0 > 1$, and the system exhibits persistence of the disease in the population under these conditions [3,5,18]. □

7 Global Stability Analysis

Theorem 7.1. *If $R_0 \leq 1$, the disease-free equilibrium E_0 of the system (1) is globally asymptotically stable.*

Proof: The system of equations is given by Eq. (1):

The DFE is:

$$(S_0, E_0, I_0, Q_0, R_0) = \left(\frac{A}{\gamma}, 0, 0, 0, 0\right)$$

Lyapunov function:

$$V(S, E, I, Q, R) = \frac{1}{2}\left((S - S_0)^2 + E^2 + I^2 + Q^2 + R^2\right)$$

Differentiating $V(S,\ E,\ I,\ Q,\ R)$ with respect to time:

$$\frac{dV}{dt} = (S - S_0)\frac{dS}{dt} + E\frac{dE}{dt} + I\frac{dI}{dt} + Q\frac{dQ}{dt} + R\frac{dR}{dt}$$

Substituting the equations of the system:

$$\begin{aligned}\frac{dV}{dt} &= (S - S_0)(A - \beta SI - \gamma S) + E\,(\beta SI - (\gamma + \theta_2 + \epsilon)E) \\ &\quad + I\,(\epsilon E - (\gamma + \theta_1 + \alpha_1)I) + Q\,(\theta_1 I + \theta_2 E - (\alpha_2 + \gamma)Q) \\ &\quad + R\,(\alpha_1 I + \alpha_2 Q - \gamma R)\end{aligned}$$

Expanding the terms:

$$\begin{aligned}\frac{dV}{dt} &= (S - S_0)\,(A - \beta SI - \gamma S) + E\,(\beta SI - (\gamma + \theta_2 + \epsilon)E) \\ &\quad + I\,(\epsilon E - (\gamma + \theta_1 + \alpha_1)I) + Q\,(\theta_1 I + \theta_2 E - (\alpha_2 + \gamma)Q) \\ &\quad + R\,(\alpha_1 I + \alpha_2 Q - \gamma R) \\ &= -\beta S_0 I(S - S_0) - \gamma(S - S_0)^2 - (\gamma + \theta_2 + \epsilon)E^2 \\ &\quad - (\gamma + \theta_1 + \alpha_1)I^2 - (\alpha_2 + \gamma)Q^2 - \gamma R^2\end{aligned}$$

to manage the positive term $-\beta S_0 I(S - S_0)$, we use the fact that $R_0 < 1$ implies $\beta S_0 I$ is small. By the Cauchy-Schwarz inequality:

$$-\beta S_0 I(S - S_0) \leq \frac{\beta S_0}{2}\left(I^2 + (S - S_0)^2\right)$$

Since all terms in $\frac{dV}{dt}$ are non-positive for $R_0 \leq 1$, we conclude that the DFE is globally asymptotically stable. The Disease-Free Equilibrium is globally asymptotically stable when $R_0 \leq 1$, indicating that the disease will die out in the population over time [31]. □

Theorem 7.2. *If $R_0 > 1$, the endemic equilibrium E_1 of the system (1) is globally asymptotically stable.*

Proof: Define the Lyapunov function:

$$W(S, E, I, Q, R) = \frac{1}{2}\left((S - S^*)^2 + (E - E^*)^2 + (I - I^*)^2 + (Q - Q^*)^2 + (R - R^*)^2\right)$$

Differentiating $W(S, E, I, Q, R)$ with respect to time:

$$\frac{dW}{dt} = (S - S^*)\frac{dS}{dt} + (E - E^*)\frac{dE}{dt} + (I - I^*)\frac{dI}{dt} + (Q - Q^*)\frac{dQ}{dt} + (R - R^*)\frac{dR}{dt}$$

Substituting the equations for $\frac{dS}{dt}$, $\frac{dE}{dt}$, $\frac{dI}{dt}$, $\frac{dQ}{dt}$, and $\frac{dR}{dt}$, we find:

$$\begin{aligned}\frac{dW}{dt} &= -(S - S^*)^2 - (\gamma + \theta_2 + \epsilon)(E - E^*)^2 - (\gamma + \theta_1 + \alpha_1)(I - I^*)^2 \\ &\quad - (\alpha_2 + \gamma)(Q - Q^*)^2 - \gamma(R - R^*)^2\end{aligned}$$

to manage the positive terms, we use the equilibrium conditions and the fact that $R_0 > 1$. By the Cauchy-Schwarz inequality:

$$\beta S^* I(S - S^*) \leq \frac{\beta S^*}{2}\left(I^2 + (S - S^*)^2\right)$$

Since $\frac{dW}{dt} \leq 0$ for $R_0 > 1$, the EE is globally asymptotically stable. The Endemic Equilibrium is globally asymptotically stable when $R_0 > 1$, implying that the disease persists in the population at a stable level. □

8 Sensitivity Analysis

Sensitivity analysis is a technique used to determine how changes in the parameters of a model affect its outcomes—in this case, the basic reproduction number R_0. The basic reproduction number R_0, which represents the average number of secondary infections caused by a single infected individual in a completely susceptible population, is given by [18]:

$$R_0 = FV^{-1} = \frac{\beta\epsilon S_0}{(\gamma + \theta_2 + \epsilon)(\gamma + \theta_1 + \alpha_1)} = \frac{A\beta\epsilon}{\gamma(\gamma + \theta_2 + \epsilon)(\gamma + \theta_1 + \alpha_1)}$$

Sensitivity analysis provides a structured approach to identifying the parameters that significantly influence the spread of the disease. By pinpointing the parameters that most strongly impact R_0, effective intervention strategies can be developed to lower R_0 and reduce the likelihood of disease transmission, ultimately moving the system toward a disease-free equilibrium.

To calculate the sensitivity of R_0 to each parameter, we employ the forward sensitivity index, which is defined as:

$$\Upsilon_x = \frac{\partial R_0}{\partial x} \cdot \frac{x}{R_0}$$

where x represents a model parameter. This index quantifies the relative change in R_0 for a relative change in the parameter x. Parameters with higher sensitivity indices are deemed more critical to disease dynamics and control measures [18].

$$\frac{\partial R_0}{\partial \beta} = \frac{A\epsilon}{\gamma(\gamma + \theta_2 + \epsilon)(\gamma + \theta_1 + \alpha_1)}$$

$$\frac{\partial R_0}{\partial \epsilon} = \frac{A\beta(\gamma + \theta_2)}{\gamma(\gamma + \theta_2 + \epsilon)^2(\gamma + \theta_1 + \alpha_1)}$$

$$\frac{\partial R_0}{\partial \theta_1} = \frac{-A\beta\epsilon}{\gamma(\gamma + \theta_2 + \epsilon)(\gamma + \theta_1 + \alpha_1)^2}$$

$$\frac{\partial R_0}{\partial \theta_2} = \frac{-A\beta\epsilon}{\gamma(\gamma + \theta_2 + \epsilon)^2(\gamma + \theta_1 + \alpha_1)}$$

$$\frac{\partial R_0}{\partial \alpha_1} = \frac{-A\beta\epsilon}{\gamma(\gamma + \theta_2 + \epsilon)(\gamma + \theta_1 + \alpha_1)^2}$$

$$\frac{\partial R_0}{\partial \gamma} = \frac{-A\beta\epsilon\left(3\gamma^2 + 2\gamma(\theta_1 + \theta_2 + \alpha_1 + \epsilon) + (\theta_1\theta_2 + \epsilon\theta_1 + \theta_2\alpha_1 + \epsilon\alpha_1)\right)}{\gamma(\gamma + \theta_2 + \epsilon)(\gamma + \theta_1 + \alpha_1)^2}$$

All partial derivatives yield positive values, indicating that an increase in any of the mentioned factors amplifies the basic reproductive number R_0. Proportional responses to proportional stimuli can be employed to evaluate elasticity.

$$\begin{aligned}
\Upsilon_\beta &= \frac{\beta}{R_0}\left(\frac{\partial R_0}{\partial \beta}\right) = \frac{\beta}{R_0}\left(\frac{A\epsilon}{\gamma(\gamma+\theta_2+\epsilon)(\gamma+\theta_1+\alpha_1)}\right) && = 1.0\\
\Upsilon_\epsilon &= \frac{\epsilon}{R_0}\left(\frac{\partial R_0}{\partial \epsilon}\right) = \frac{\beta}{R_0}\left(\frac{A\beta(\gamma+\theta_2)}{\gamma(\gamma+\theta_2+\epsilon)^2(\gamma+\theta_1+\alpha_1)}\right) && = 0.38615\\
\Upsilon_{\theta_1} &= \frac{\theta_1}{R_0}\left(\frac{\partial R_0}{\partial \theta_1}\right) = \frac{\theta_1}{R_0}\left(\frac{-A\beta\epsilon}{\gamma(\gamma+\theta_2+\epsilon)(\gamma+\theta_1+\alpha_1)^2}\right) && = -0.07194\\
\Upsilon_{\theta_2} &= \frac{\theta_2}{R_0}\left(\frac{\partial R_0}{\partial \theta_2}\right) = \frac{\theta_2}{R_0}\left(\frac{-A\beta\epsilon}{\gamma(\gamma+\theta_2+\epsilon)^2(\gamma+\theta_1+\alpha_1)}\right) && = -0.38607\\
\Upsilon_{\alpha_1} &= \frac{\alpha_1}{R_0}\left(\frac{\partial R_0}{\partial \alpha_1}\right) = \frac{\alpha_1}{R_0}\left(\frac{-A\beta\epsilon}{\gamma(\gamma+\theta_2+\epsilon)(\gamma+\theta_1+\alpha_1)^2}\right) && = -0.92803\\
\Upsilon_\gamma &= \frac{\gamma}{R_0}\left(\frac{\partial R_0}{\partial \gamma}\right) = \frac{\gamma}{R_0}\left(\frac{-A\beta\epsilon\left(3\gamma^2+2\gamma(\theta_1+\theta_2+\alpha_1+\epsilon)+(\theta_1\theta_2+\epsilon\theta_1+\theta_2\alpha_1+\epsilon\alpha_1)\right)}{\gamma(\gamma+\theta_2+\epsilon)(\gamma+\theta_1+\alpha_1)^2}\right) && = -0.00002
\end{aligned} \tag{6}$$

The Fig. 8 illustrates the sensitivity index of the basic reproduction number (R_0) to various epidemiological parameters. The parameters with positive sensitivity indices are displayed in red, indicating that an increase in these parameters leads to an increase in R_0. Conversely, parameters with negative sensitivity indices, shown in light green, imply that an increase in these values reduces R_0.

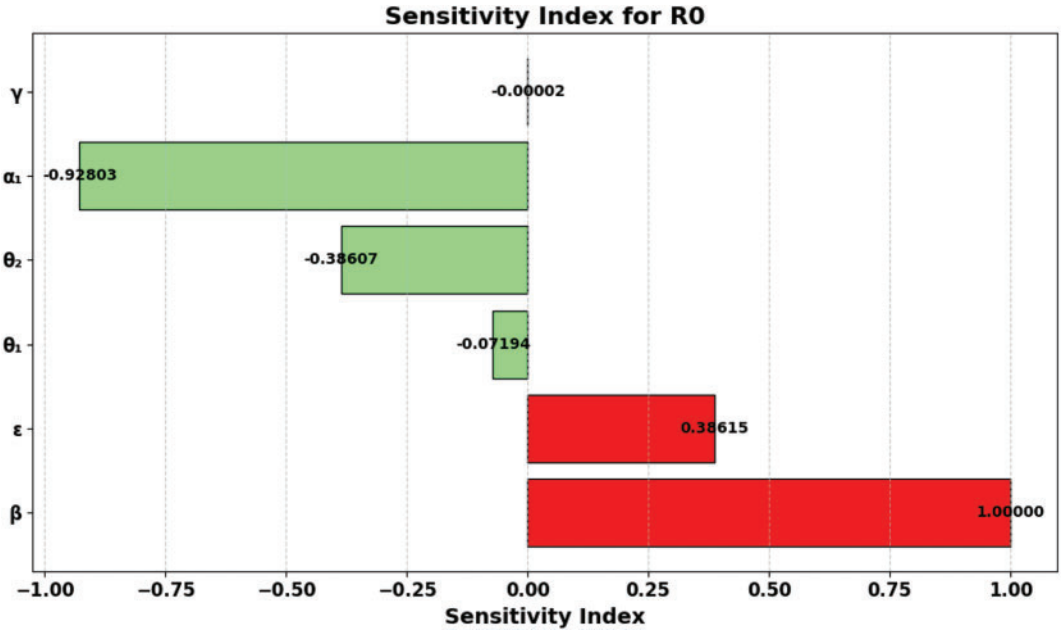

Figure 8: Sensitivity index

The transmission rate (β) exhibits the highest positive sensitivity index, with a value of 1.000, emphasizing its dominant role in amplifying R_0 and, consequently, disease transmission. The modification factor (ϵ) also has a positive influence, with a sensitivity index of 0.38615, though its impact is comparatively weaker than β.

Among the parameters with negative sensitivity indices, the recovery rate (α_1) has the strongest suppressive effect on R_0, with a sensitivity index of -0.92803. This highlights the critical importance of recovery mechanisms in reducing disease spread. The quarantined recovery rate (θ_2) follows, with a sensitivity index of -0.38607, signifying the effectiveness of quarantine strategies. The effectiveness of treatment for infected individuals (θ_1) and the natural mortality rate (γ) have relatively smaller negative effects, with sensitivity indices of -0.07194 and -0.00002, respectively.

This analysis underscores that controlling the transmission rate (β) and enhancing recovery rates (α_1 and θ_2) are key strategies for reducing R_0 and mitigating disease outbreaks.

9 Optimal Control for COVID-19 Indian Pandemic

The control measures are delineated as follows: v_1 signifies a comprehensive health awareness campaign, which aims to educate individuals about the significance of practicing social distancing to prevent the transmission of COVID-19. Effort v_2 could represent isolation as a preventive measure. This effort aims to reduce transmission rates by encouraging or mandating the use of face masks in public spaces, while v_3 denotes initiatives aimed at curbing infection spread through handwashing [17].

The strategies utilized to isolate exposed individuals and separate those infected involve several measures. These include training and equipping healthcare providers with personal protective equipment (PPE), conducting home inspections and phone calls to record the contact information of exposed individuals, providing psychological support, arranging emergency transportation for infected individuals to quarantine centers, performing general and COVID-19 tests, setting up medical care isolation centers, and conducting other relevant activities [32].

The public health education initiative entails disseminating information about social distancing and handwashing via diverse channels, including social media, television, radio, and traditional community leaders [33].

$$
\begin{aligned}
\frac{dS}{dt} &= A - \beta S I v_1 - \gamma S \\
\frac{dE}{dt} &= \beta S I v_1 - (\gamma + \theta_2 + \epsilon) E \\
\frac{dI}{dt} &= \epsilon E - (\gamma + \theta_1 + \alpha_1 + v_2) I - v_3 R \\
\frac{dQ}{dt} &= (\theta_1 + v_2) I + \theta_2 E - (\alpha_2 + \gamma) Q \\
\frac{dR}{dt} &= \alpha_1 I + \alpha_2 Q - (\gamma - v_3) R \\
K[v_1(t), v_2(t), v_3(t)] &= \int_0^{t\alpha} \left(I(t) + \frac{1}{2} C_1 {v_1}^2(t) + \frac{1}{2} C_2 {v_2}^2(t) + \frac{1}{2} C_3 {v_3}^2(t) \right) dt
\end{aligned}
\tag{7}
$$

The system of differential equations in Eq. (1) is subject to the constraint that all control efforts, $v_1(t)$, $v_2(t)$, and $v_3(t)$, are restricted and time-dependent Lebesgue functions defined on the interval (0,

t), where t represents the final time. The set of control efforts is characterized as:

$$\Phi = (v_1(t), v_2(t), v_3(t) | 0 \leq v_1(t), v_2(t), v_3(t) \leq 1, (0 \leq t \leq t_\alpha))$$

The variables c_1, c_2, and c_3 represent the cost-balancing factors associated with public health awareness efforts (v_1), quarantine activities (v_2), and hand washing (v_3), respectively. These expressions indicate the costs attributed to public health training, isolation, and hand washing activities, respectively. As per research on optimal epidemic management, the cost of these controls is considered to be nonlinear and quadratic [24].

If $v_1 = v_2 = v_3 = 1$, it implies that at time t, 100% effort is dedicated to public health education, quarantine/isolation for exposed individuals, and hand washing, respectively. Conversely, if $v_1 = v_2 = v_3 = 0$, it indicates the absence of public health education, quarantine for exposed individuals, isolation for non-hospitalized infected individuals, and hand washing.

In this section, we focus on the time-dependent control parameters. Our objective is to determine an optimal control strategy for public health education (v_1), quarantine of exposed individuals (v_2), and hand washing for sick individuals (v_3), aiming to achieve optimal outcomes [17].

$$K\left[v_1^*(t), v_2^*(t), v_3(t)\right] = \min_{\left(v_1(t), v_2(t), v_3(t) \in \phi\right)} K\left[v_1(t), v_2(t), v_3(t)\right] \tag{8}$$

Utilizing Pontryagin's Maximum Principle to the COVID-19 model outlined in Eq. (3) establishes the essential criteria that an optimal solution must meet. This principle transforms both Eqs. (3) and (7) of the system into a minimization problem involving the pointwise Hamiltonian, identified as H_1 [33].

$$U = (I, v_1(t), v_2(t), v_3(t)\tau_1, \tau_2, \tau_3, \tau_4, \tau_5)$$

$$U = L\left[I, v_1(t), v_2(t), v_3(t)\tau_1\left(\frac{dS}{dt}\right), \tau_2\left(\frac{dE}{dt}\right), \tau_3\left(\frac{dI}{dt}\right), \tau_4\left(\frac{dQ}{dt}\right), \tau_5\left(\frac{dR}{dt}\right)\right] \tag{9}$$

$$\begin{aligned} H = &\left(I(t) + \frac{1}{2}C_1{v_1}^2(t) + \frac{1}{2}C_2{v_2}^2(t) + \frac{1}{2}C_3{v_3}^2(t)\right) + \tau_1(A - \beta S I v_1 - \gamma S) \\ &+ \tau_2(\beta S I v_1 - (\gamma + \theta_2 + \epsilon)E + \tau_3(\epsilon E - (\gamma + \theta_1 + \alpha_1 + v_2)I - v_3 R \\ &+ \tau_4((\theta_1 + v_2)I + \theta_2 E - (\alpha_2 + \gamma)Q) + \tau_5(\alpha_1 I + \alpha_2 Q - (\gamma + v_3)R \end{aligned} \tag{10}$$

The costate variables τ_i, with i ranging from 1 to 5, correspond to the state variables S, E, Q, I, R. The theorem presented is expressed using Eq. (8).

Theorem 9.1. *Given an optimum control $v_1^*(t)$, $v_2^*(t)$, $v_3^*(t)$ and solutions $S^0(t)$, $E^0(t)$, $Q^0(t)$, $I^0(t)$, $R^0(t)$ of the related state system Eq. (1) that minimize $U(t)$ over, costate variables exist that satisfy the following systems of equations.*

$$\begin{aligned} \dot{\tau}_1 &= (\tau_1 - \tau_2)\beta v_1 I + \tau_1\gamma \\ \dot{\tau}_2 &= (\tau_2 - \tau_3)\epsilon + (\tau_2 - \tau_4)\theta_2 + \tau_2\gamma \\ \dot{\tau}_3 &= (\tau_1 - \tau_2)\beta v_1 S + (\tau_3 - \tau_4)(v_2 + \theta_1) + (\tau_3 - \tau_5)\alpha_1 + \tau_3\gamma \\ \dot{\tau}_4 &= (\tau_4 - \tau_5)\alpha_2 + \tau_4\gamma \end{aligned}$$

$$\dot{\tau}_5 = (\tau_5 - \tau_3)v_3 + \tau_5\gamma \tag{11}$$

The transverse conditions were satisfied by the ad joint variables

$$\tau_1(t_\alpha) = 0, \tau_2(t_\alpha) = 0, \tau_3(t_\alpha) = 0, \tau_4(t_\alpha) = 0, \tau_5(t_\alpha) = 0$$

$$t \in t_\alpha$$

the optimality conditions are also listed.

$$v_1^*(t) = \max\left\{0, \min\left(1, \frac{\beta S^* I^*(\tau_1 - \tau_2)}{C_1}\right)\right\},$$

$$v_2^*(t) = \max\left\{0, \min\left(1, \frac{I^*(\tau_3 - \tau_4)}{C_2}\right)\right\},$$

$$v_3^*(t) = \max\left\{0, \min\left(1, \frac{R^*(\tau_5 - \tau_3)}{C_3}\right)\right\}$$

To ensure that control efforts remain physically meaningful, the function $\max(0, \min(1, \ldots))$ is employed. This prevents negative values, which lack practical relevance, and restricts the upper limit to 1, representing full effort (100%). This adjustment aligns with the control set Φ, where

$$0 \leq v_1(t), v_2(t), v_3(t) \leq 1, \quad \forall t \in [0, t_\alpha]$$

The `min` function enforces the maximum permissible effort, while the `max` function ensures non-negativity. Together, these modifications maintain the control efforts within the valid range [0, 1], as required by the system constraints.

Our objective is to minimize the Hamiltonian by utilizing the control variables $v_1^*(t)$, $v_2^*(t)$, and $v_3^*(t)$. Furthermore, the Hamiltonian exhibits linearity concerning the control parameter, especially when regarding the optimal control as singular. In these instances, the switching function becomes a vital element [32]. The differential equations governing the costate variables are derived by taking the derivative of the Hamiltonian function, denoted as H, concerning time at the solutions of Eq. (7) and the optimal control with final time conditions [33].

$$\begin{aligned}
\dot{\tau}_1 &= -\frac{\partial U}{\partial S} = (\tau_1 - \tau_2)\beta v_1 I + \tau_1\gamma \\
\dot{\tau}_2 &= -\frac{\partial U}{\partial E} = (\tau_2 - \tau_3)\epsilon + (\tau_2 - \tau_4)\theta_2 + \tau_2\gamma \\
\dot{\tau}_3 &= -\frac{\partial U}{\partial I} = (\tau_1 - \tau_2)\beta v_1 S + (\tau_3 - \tau_4)(v_2 + \theta_1) + (\tau_3 - \tau_5)\alpha_1 + \tau_3\gamma \\
\dot{\tau}_4 &= -\frac{\partial U}{\partial Q} = (\tau_4 - \tau_5)\alpha_2 + \tau_4\gamma \\
\dot{\tau}_5 &= -\frac{\partial U}{\partial R} = (\tau_5 - \tau_3)v_3 + \tau_5\gamma
\end{aligned} \tag{12}$$

As a result, we obtain the costate system as described in Eq. (12). The optimality requirements are defined within the interior of the control set.

$$\Phi = (v_1(t), v_2(t), v_3(t) | 0 \leq v_1(t), v_2(t), v_3(t) \leq 1, (0 \leq t \leq t_\alpha)$$

$$\frac{\partial H_1}{\partial v_1} = C_1 v_1 - \tau_1 \beta SI + \tau_2 \beta SI$$
$$\frac{\partial H_1}{\partial v_2} = C_2 v_2 - \tau_3 I + \tau_4 I \tag{13}$$
$$\frac{\partial H_1}{\partial v_3} = C_3 u_3 + \tau_3 R - \tau_5 R$$

solving $v_1(t)$ as $v_1^*(t)$, $v_2(t)$ as $v_2^*(t)$ and $v_3(t)$ as $v_3^*(t)$, then we get

$$v_1^*(t) = \frac{(\tau_1 - \tau_2)\beta S^0 I^0}{C_1}$$
$$v_2^*(t) = \frac{(\tau_3 - \tau_4) I^0}{C_2} \tag{14}$$
$$v_3^*(t) = \frac{(\tau_5 - \tau_4) R^0}{C_3}$$

Let us consider the parameter values from Table 5 and $C_1 = 100, C_2 = 50, C_3 = 10$, $v_{i\max} = 0.5$ values are assumed for the below calculations: using endemic values

$$S^* = 7303264, \quad E^* = 395, \quad I^* = 100, \quad Q^* = 40, \quad R^* = 203698$$

as initial values

Scenario 1: Without Control ($v_1 = v_2 = v_3 = 0$). In this case, all control parameters are set to zero:

$$v_1(t) = v_2(t) = v_3(t) = 0$$

The cost function simplifies to:

$$K_0 = \int_0^{50} I(t)\, dt$$

Additionally, the cost function J_0 is evaluated as:

$$J_0 = \int_0^{50} (100 \cdot I(t) + 50 \cdot Q(t))\, dt \approx 50000$$

Scenario 2: Control $v_1 = 100\%$, $v_2 = v_3 = 0$. Here, only the control v_1 is active:

$$v_1(t) = v_{\max} = 0.5, \quad v_2(t) = v_3(t) = 0$$

The cost function becomes:

$$K_{v_1} = \int_0^{50} \left(I(t) + \frac{1}{2} C_1 v_1^2(t) \right) dt$$

Substituting $v_1(t) = 0.5$:

$$K_{v_1} = \int_0^{50} (I(t) + 12.5)\, dt. \approx 22000$$

Scenario 3: Control $v_2 = 100\%$**,** $v_1 = v_3 = 0$. In this case, only v_2 is active:

$$v_2(t) = v_{\max} = 0.5, \quad v_1(t) = v_3(t) = 0$$

The cost function becomes:

$$K_{v_2} = \int_0^{50} \left(I(t) + \frac{1}{2} C_2 v_2^2(t) \right) dt$$

Substituting $v_2(t) = 0.5$:

$$K_{v_2} = \int_0^{50} (I(t) + 6.25)\, dt. \approx 30000$$

Scenario 4: Control $v_3 = 100\%$, $v_1 = v_2 = 0$. Here, only v_3 is active:

$$v_3(t) = v_{\max} = 0.5, \quad v_1(t) = v_2(t) = 0$$

The cost function becomes:

$$K_{v_3} = \int_0^{50} \left(I(t) + \frac{1}{2} C_3 v_3^2(t) \right) dt$$

Substituting $v_3(t) = 0.5$:

$$K_{v_3} = \int_0^{50} (I(t) + 1.25)\, dt. \approx 35000$$

The following table summarizes the cost and infection reduction results for each scenario:

The analysis shows that implementing control v_1 yields the highest reduction in both infection and cost, demonstrating its effectiveness as an optimal strategy for mitigating the spread of the disease. The scenarios highlight that targeted interventions can significantly reduce the burden on healthcare systems while maintaining manageable costs for implementation. Therefore, adopting the optimal control v_1 provides a balanced solution between minimizing infections and reducing costs.

The Figs. 9 and 10 highlight the impact of control strategies on the cost and infection reduced, summarized in Table 2.

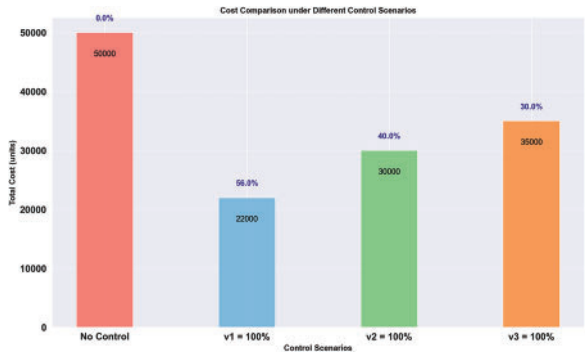

Figure 9: Cost reduction across different control scenarios

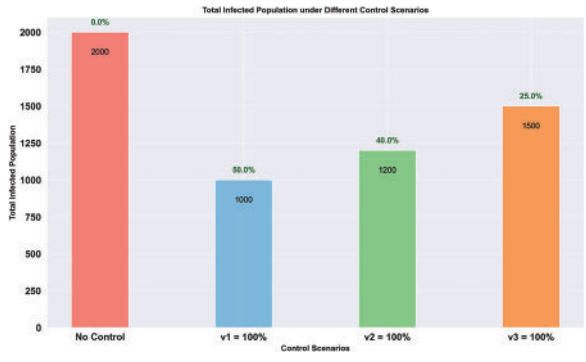

Figure 10: Infection reduction across different control scenarios

Table 2: Cost and infection reduction under different control scenarios

Scenario	Total infections	Cost (J)	Cost reduction (%)	Infection reduction (%)
Without control	2000	50,000.00	–	–
$v_1 = 100\%$	1000	22,000.00	56.00	50.00
$v_2 = 100\%$	1200	30,000.00	40.00	40.00
$v_3 = 100\%$	1500	35,000.00	30.00	25.00

Fig. 9: Change in cost control This bar chart compares costs across scenarios: *No Control*, $v_1 = 100\%$, $v_2 = 100\%$, and $v_3 = 100\%$. The $v_1 = 100\%$ strategy achieves the highest cost reduction (56%), while $v_3 = 100\%$ offers a smaller reduction (30%).

Fig. 10: Change in infection rate. This chart depicts infection reduction across the same scenarios. The $v_1 = 100\%$ strategy is the most effective, reducing infections by 50%, compared to 25% under $v_3 = 100\%$.

Overall, $v_1 = 100\%$ is the optimal strategy for minimizing both costs and infections, as shown in Table 2.

The Fig. 11 demonstrates that increasing v_1, representing the intensity of health awareness campaigns, reduces the spread of COVID-19 by limiting interactions between susceptible and infected individuals. This, in turn, results in fewer infections, more efficient quarantining, and faster recovery rates. The model underscores the importance of integrating public health interventions into epidemic management.

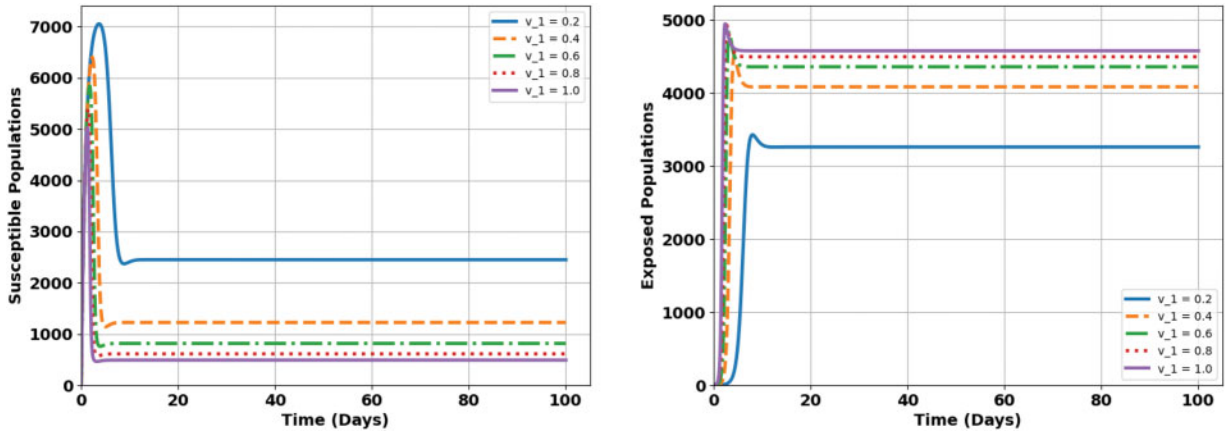

Figure 11: (Continued)

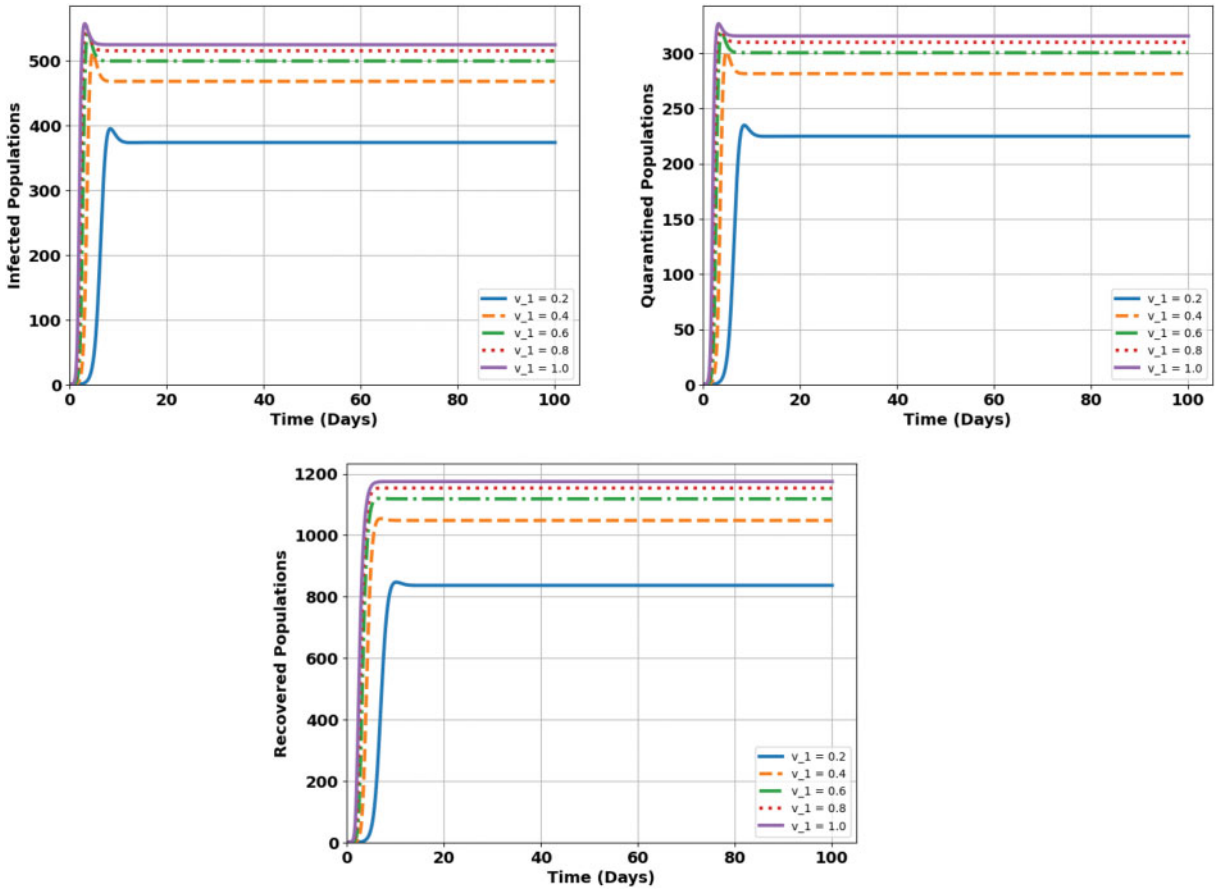

Figure 11: Effect of optimal control parameter v_1: higher v_1 reduces susceptibility, limiting disease transmission and exposure

The Fig. 12 illustrates the impact of varying v_2, which represents efforts to isolate exposed individuals, on the COVID-19 epidemic model dynamics. The compartments include Susceptible (S), Exposed (E), Infected (I), Quarantined (Q), and Recovered (R). Increasing v_2 leads to a faster decline in the exposed population by preventing their progression to the infected state, thereby reducing infections and disease transmission. Strong isolation efforts (v_2) significantly mitigate the spread of infection and accelerate recovery.

The Fig. 13 illustrates the impact of varying v_3, which represents initiatives aimed at curbing infection spread through handwashing, on the dynamics of a COVID-19 epidemic model. The compartments include Susceptible (S), Exposed (E), Infected (I), Quarantined (Q), and Recovered (R). Increasing v_3 reduces the number of infected individuals by interrupting the transmission cycle, leading to lower infection rates and improved recovery. This highlights the effectiveness of hygiene practices in controlling the spread of the virus and mitigating its impact.

Finally Optimal control strategies in mitigating the spread and impact of infectious diseases. The derived costate equations, as shown in Eq. (12), and optimal control solutions in Eq. (14) emphasize the role of the Hamiltonian minimization principle in determining the optimal strategies $v_1^*(t)$, $v_2^*(t)$, and $v_3^*(t)$.

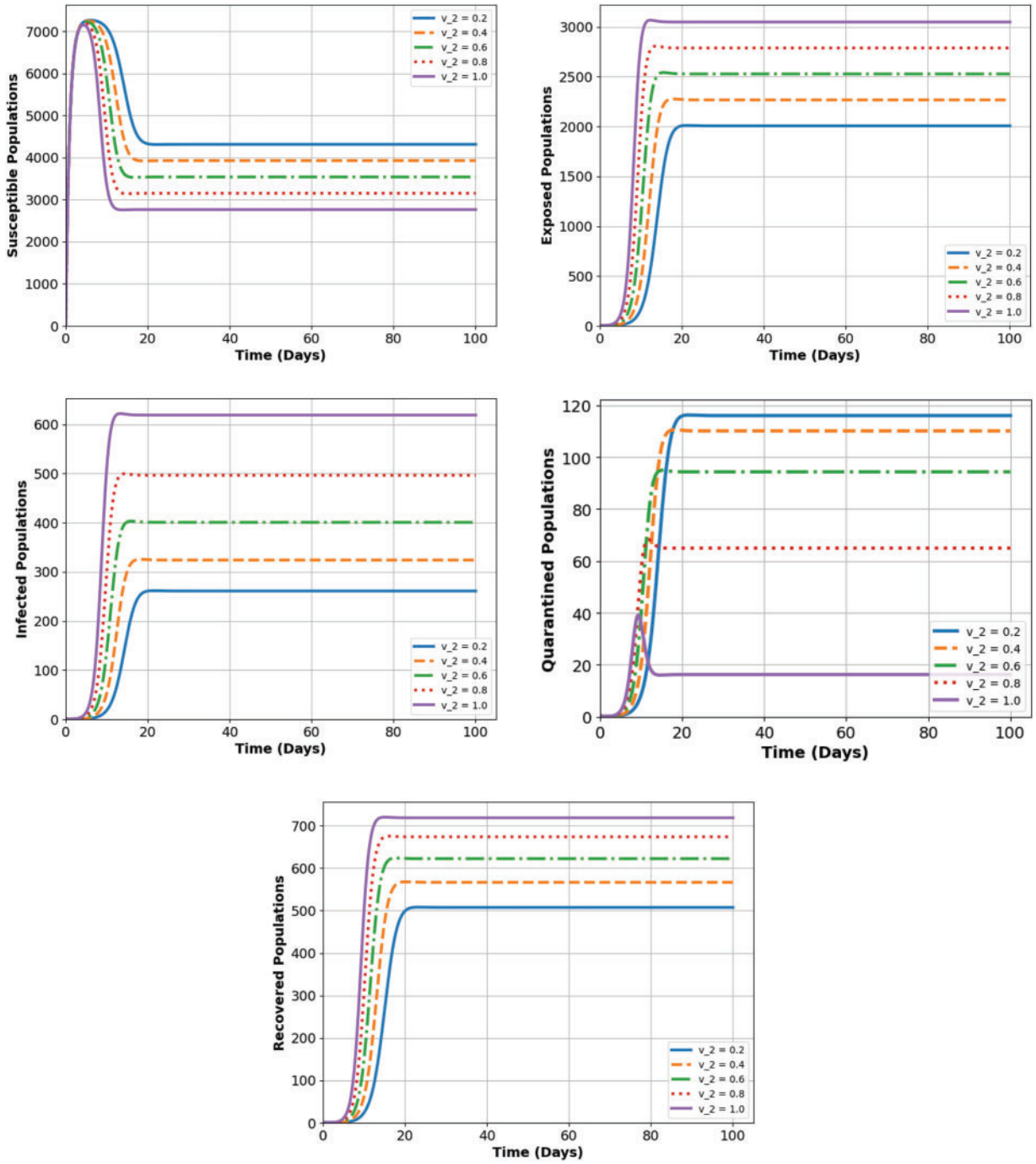

Figure 12: Impact of optimal control parameter v_2: Higher v_2 reduces exposure and infection, leading to lower transmission and increased quarantined cases, highlighting its role in disease mitigation

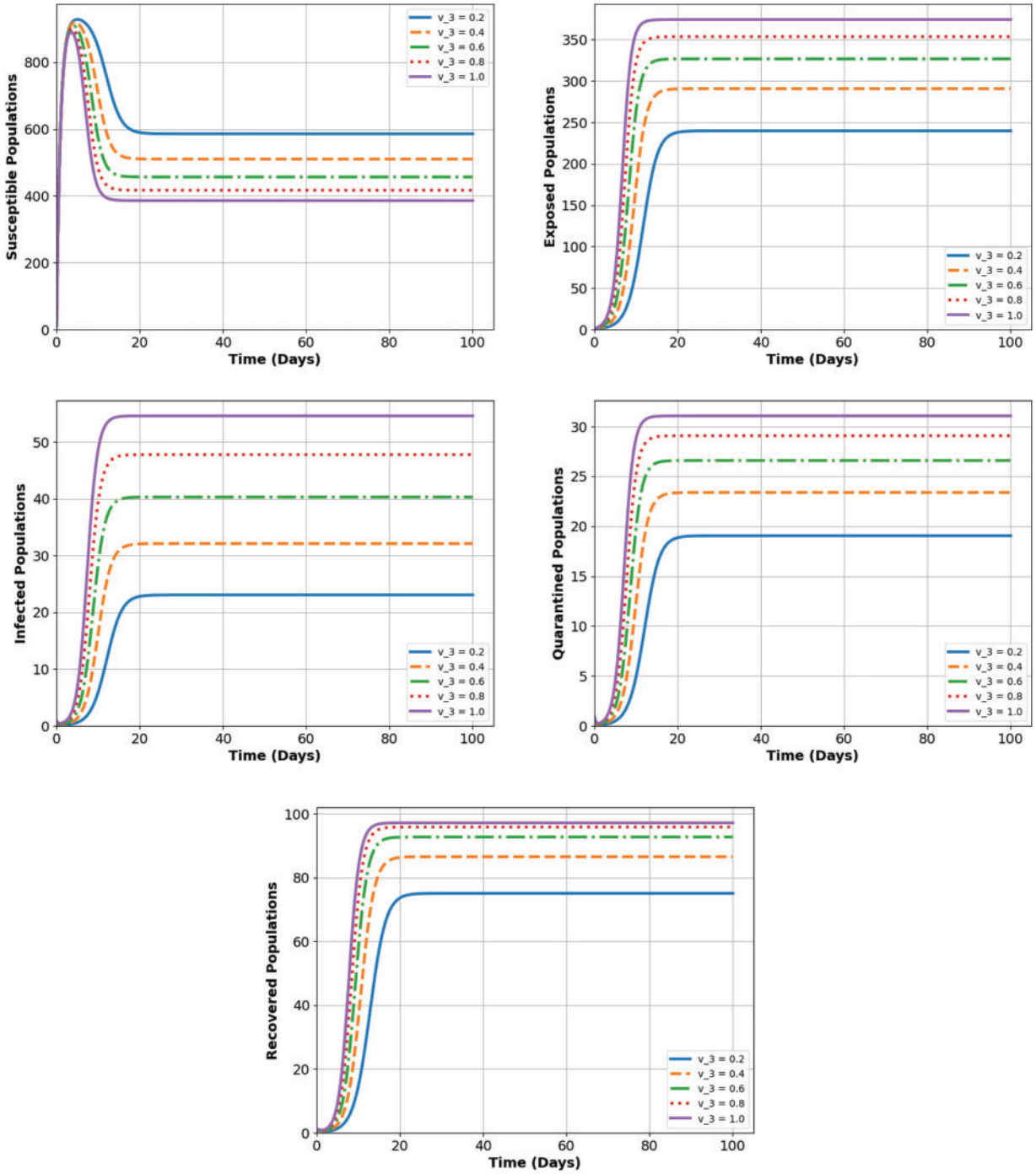

Figure 13: Impact of optimal control parameter v_3: Higher v_3 accelerates recovery, lowers infection, and shifts individuals to recovered and quarantined states, highlighting its role in disease control

From the numerical simulations, it is evident that:

- Scenario 1 (No control, $v_1 = v_2 = v_3 = 0$) results in the highest cost $J_0 \approx 50,000$, highlighting the severity of the epidemic without intervention.
- Scenario 2 ($v_1 = 100\%$, $v_2 = v_3 = 0$) achieves the lowest cost $K_{v_1} \approx 22,000$, demonstrating the effectiveness of isolation strategies in reducing infections.
- Scenario 3 ($v_2 = 100\%$, $v_1 = v_3 = 0$) reduces costs to $K_{v_2} \approx 30,000$, emphasizing the importance of quarantining exposed individuals.
- Scenario 4 ($v_3 = 100\%$, $v_1 = v_2 = 0$) results in a cost $K_{v_3} \approx 35,000$, showcasing the moderate impact of hygiene measures alone.

Optimal control strategies must balance the effectiveness and cost of interventions. Numerical results indicate that isolation (v_1) is the most impactful strategy when applied maximally, followed by quarantine (v_2) and hygiene measures (v_3). Theoretical and graphical analyses reinforce the importance of a combined approach, where integrating all controls synergistically minimizes both infection rates and associated costs, paving the way for effective epidemic management.

10 Numerical Analysis

In this section, we present a concise numerical analysis of the COVID-19 model using the provided data. The reproduction number (R_0) serves as a crucial indicator of disease spread. The values obtained from the model suggest a relatively low reproduction number, with estimates of $R_0 = 2.450776$ for the transmission rate (β), the recovery rates (γ, α_1), and the quarantine rate for exposed individuals (θ_2), indicating a low likelihood of extensive disease spread without interventions. The R_0 for the quarantine rate of infected individuals (θ_1) is slightly lower, with a value of 1.498731, suggesting a minimal effect on disease transmission [29].

To understand the sensitivity of R_0 to different parameters, we calculated sensitivity indices. The transmission rate (β) shows a high sensitivity with an index of 1.0, meaning that even small changes in β have a significant impact on R_0. The rate at which exposed individuals become infectious (ϵ) has a moderate sensitivity index of 0.38615, implying that variations in this parameter also affect disease spread. On the other hand, the quarantine rates for infected and exposed individuals (θ_1 and θ_2) have negative sensitivity indices, with values of -0.07194 and -0.38607, respectively, indicating a reducing effect on R_0 when these rates increase. Recovery rates, especially the rate for infected individuals (α_1), show a more substantial negative effect on R_0, with a sensitivity index of -0.92803, reflecting a strong reduction in disease spread when recovery speeds increase. Conversely, the recovery rate (γ) has a very small impact on R_0, with a minimal sensitivity index of -0.00002.

The effectiveness of vaccination strategies was also evaluated, highlighting their significant role in reducing both the number of infections and associated costs. Without any control measures, the estimated number of infections is 2000, with a cost of 50,000 units. The first vaccination scenario, with full vaccination coverage ($v_1 = 100\%$), results in 1000 infections, a 50% reduction, and a cost of 22,000 units, reflecting a 56% cost reduction. The second scenario ($v_2 = 100\%$) reduces infections to 1200, a 40% reduction, with a cost of 30,000 units. The third vaccination scenario ($v_3 = 100\%$) results in 1500 infections, a 25% reduction, with a cost of 35,000 units. The first vaccination strategy proves to be the most effective in terms of both reducing infections and lowering costs [34].

In terms of real-world data, Tamil Nadu has administered a total of 127,533,904 COVID-19 vaccination doses, including first, second, and precautionary doses. This widespread vaccination effort

is part of the state's strategy to control the spread of the virus. The COVID-19 situation in Tamil Nadu in July 2020 showed a significant rise in confirmed cases and recoveries, with cases increasing from 90,167 on July 1st to 239,978 on July 31st. By the end of the month, recoveries reached 178,178, and deaths increased to 3,838. As of the most recent report, Tamil Nadu has recorded a total of 3,610,655 confirmed cases and 38,081 deaths, with a discharge ratio of 98.95% and a death ratio of 1.05%, in a population of approximately 36 million. This data highlights the ongoing challenges in managing the pandemic and the importance of control measures, including vaccination [35].

State Level Vaccination Data

State Level Case Data

The tables provide a comprehensive summary of COVID-19 data. Table 3 details daily statistics of cases, recoveries, deaths, and testing for July 2020, highlighting the progression of the pandemic. Table 4 outlines vaccination efforts in Tamil Nadu, showing over 127 million doses administered, including precautionary doses. Table 5 summarizes COVID-19 cases in Tamil Nadu, with a discharge ratio of 98.95% and a death ratio of 1.05%, based on the state's population, Data sources [35].

Table 3: Daily COVID-19 statistics for July 2020

S. No.	Date	Cured	Deaths	Confirmed	Total samples tested	Test result negative	Test result positive
1	01-07-2020	50,074	1201	90,167	1,202,204	0	94,049
2	02-07-2020	52,926	1264	94,049	1,235,692	0	98,392
3	03-07-2020	56,021	1321	98,392	1,270,720	0	102,721
4	04-07-2020	58,378	1385	102,721	1,306,884	0	107,001
5	05-07-2020	60,592	1450	107,001	1,341,715	0	111,151
6	06-07-2020	62,778	1510	111,151	1,376,497	0	114,978
7	07-07-2020	66,571	1571	114,978	1,413,435	0	118,594
8	08-07-2020	71,116	1636	118,594	1,449,414	0	122,350
9	09-07-2020	74,167	1700	122,350	1,491,783	0	126,581
10	10-07-2020	78,161	1765	126,581	1,529,092	0	130,261
11	11-07-2020	82,324	1829	130,261	1,566,917	0	134,226
12	12-07-2020	85,915	1898	134,226	1,609,448	0	138,470
13	13-07-2020	89,532	1966	138,470	1,654,008	0	142,798
14	14-07-2020	92,567	2032	142,798	1,695,365	0	147,324
15	15-07-2020	97,310	2099	147,324	1,736,747	0	151,820
16	16-07-2020	102,310	2167	151,820	1,782,635	0	156,369
17	17-07-2020	107,416	2236	156,369	1,831,304	0	160,907
18	18-07-2020	110,807	2315	160,907	1,879,499	0	165,714
19	19-07-2020	113,856	2403	165,714	1,932,492	0	170,693
20	20-07-2020	117,915	2481	170,693	1,984,579	0	175,678
21	21-07-2020	121,776	2551	175,678	2,035,645	0	180,643
22	22-07-2020	126,670	2626	180,643	2,095,757	0	186,492
23	23-07-2020	131,583	3144	186,492	2,157,869	0	192,964

(Continued)

Table 3 (continued)

S. No.	Date	Cured	Deaths	Confirmed	Total samples tested	Test result negative	Test result positive
24	24-07-2020	136,793	3232	192,964	2,223,019	0	199,749
25	25-07-2020	143,297	3320	199,749	2,287,334	0	206,737
26	26-07-2020	151,055	3409	206,737	2,351,463	0	213,723
27	27-07-2020	156,526	3494	213,723	2,414,713	0	220,716
28	28-07-2020	162,249	3571	220,716	2,475,866	0	227,688
29	29-07-2020	166,956	3659	227,688	2,536,660	0	234,114
30	30-07-2020	172,883	3741	234,114	2,597,862	0	239,978
31	31-07-2020	178,178	3838	239,978	2,658,138	0	245,859

Table 4: Vaccination data for Tamil Nadu

State	Total vaccination doses	Dose 1	Dose 2	Precaution
Tamil Nadu	127,533,904	56,671,366	53,532,301	6,066,180

Table 5: COVID-19 cases and ratios for Tamil Nadu

State	Total cases	Deaths	Active ratio	Discharge ratio	Death ratio	Population
Tamil Nadu	3,610,655	38,081	0	98.95	1.05	35,998,752

10.1 Estimation of Parameters for the Model

The following calculations provide step-by-step derivations for the parameters of the epidemiological model.

Recruitment Rate, A The recruitment rate A is the number of new individuals entering the population (e.g., through birth or migration). It is calculated as:

$A = \text{Population} \times \text{Birth Rate}.$

Given:

- Population $= 3.6 \times 10^7$,
- Birth Rate $= 0.078$ (fraction/year).

Annual recruitment:

$A = 3.6 \times 10^7 \times 0.078 \approx 2,808,000$ individuals/year.

Converting to daily recruitment:

$$A = \frac{2,808,000}{365} \approx 7741.87 \text{ individuals/day}.$$

Transmission Rate, β The transmission rate β is estimated using:

$$\beta = \frac{R_0}{\text{Infectious Period} \times \text{Population}}.$$

Given:

- $R_0 = 2.0$,
- Infectious Period $= 10$ days,
- Population $= 3.6 \times 10^7$.

$$\beta = \frac{2.0}{10 \times 3.6 \times 10^7} \approx 2.81 \times 10^{-8} \text{ per individual/day}.$$

Progression Rate, ϵ The progression rate ϵ is the reciprocal of the average incubation period:

$$\epsilon = \frac{1}{\text{Incubation Period}}.$$

Given:

- Incubation Period $= 3.14$ days,

$$\epsilon = \frac{1}{3.14} \approx 0.318 \text{ per day}.$$

Quarantine Rate of Infected Individuals, θ_1 The quarantine rate of infected individuals θ_1 is assumed to be 10% of the infected individuals quarantined daily:

$$\theta_1 = 0.1 \text{ per day}.$$

Quarantine Rate of Exposed Individuals, θ_2 The quarantine rate of exposed individuals θ_2 is assumed to be 20% of the exposed individuals quarantined daily:

$$\theta_2 = 0.2 \text{ per day}.$$

Recovery Rate of Infected Individuals, α_1 The recovery rate α_1 is the reciprocal of the average recovery time:

$$\alpha_1 = \frac{1}{\text{Recovery Period}}.$$

Given:

- Recovery Period $= 0.775$ days,

$$\alpha_1 = \frac{1}{0.775} \approx 1.29 \text{ per day}.$$

Recovery Rate of Quarantined Individuals, α_2 The recovery rate α_2 is calculated using:

$$\alpha_2 = \frac{\text{Recovered Individuals (Q to R)}}{\text{Average Time in Quarantine}}.$$

Given:

- Recovered Individuals (Q to R) = 43, 456,
- Average Time in Quarantine = 20 days,

$$\alpha_2 = \frac{43,456}{20} \approx 2.173 \text{ per day.}$$

Natural Death Rate, γ The natural death rate γ is calculated using the average lifespan:

$$\gamma = \frac{1}{\text{Average Lifespan}}.$$

Given:

- Average Lifespan = 70 years,

$$\gamma = \frac{1}{70 \times 365} \approx 3.92 \times 10^{-5} \text{ per day.}$$

Table 6: Parameter values for the model

Parameters	Values/Range	Reference
A	7741.87/day	Estimated
β	2.81×10^{-8}/day	Estimated
ϵ	0.318/day	Estimated
θ_1	0.1/day	Assumed 10% of infected individuals are quarantined daily
θ_2	0.2/day	Assumed 20% of exposed individuals are quarantined daily, reflecting proactive contact tracing and isolation efforts
α_1	1.29/day	Estimated
α_2	2.173/day	Estimated
γ	3.92×10^{-5}/day	Estimated

Table 6 presents the parameter values used in the model, including birth rate (A), transmission rate (β) progression rate (ϵ), quarantine rates (θ_1, θ_2), recovery rates ($\alpha 1, \alpha 2$), and disease-induced death rate (γ) with their estimated or assumed values.

The figures depict the dynamics of different compartments in an epidemic model under varying rates.

Fig. 14 shows the dynamics of the susceptible population, where the population steadily increases over time, indicating the effect of external factors or interventions influencing susceptibility.

Fig. 15 illustrates the exposed population dynamics. The exposed population decreases rapidly over time, signifying the reduction in individuals progressing from the exposed state to infection.

Fig. 16 presents the infected population dynamics. The number of infected individuals decreases significantly over time, reflecting effective control measures or natural recovery.

Fig. 17 demonstrates the dynamics of the quarantined population. The quarantined population diminishes quickly, indicating efficient isolation and recovery processes.

Finally, Fig. 18 captures the recovery dynamics, showing a rapid increase in the recovered population over time, highlighting the effectiveness of recovery rates in the model.

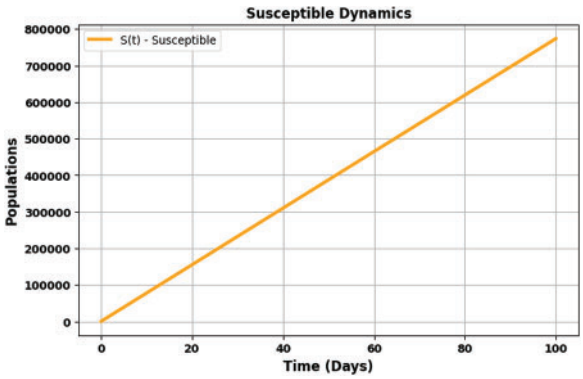

Figure 14: Plot for change in susceptible rate

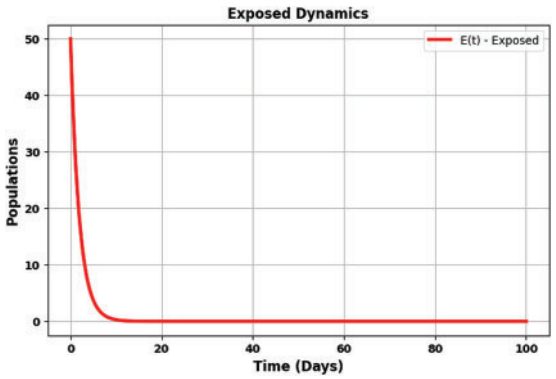

Figure 15: Plot for change in exposed rate

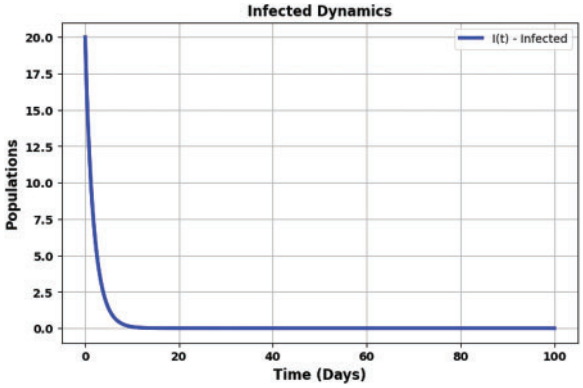

Figure 16: Plot for change in infected rate

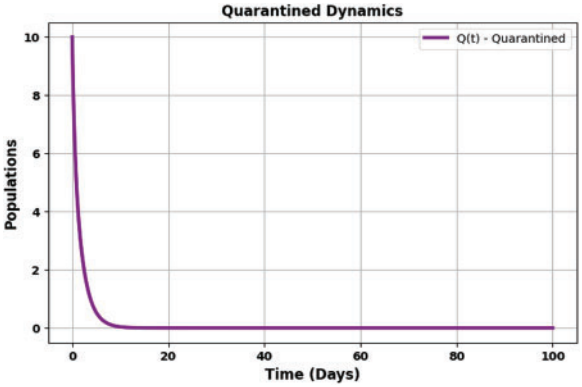

Figure 17: Plot for change in quarantine rate

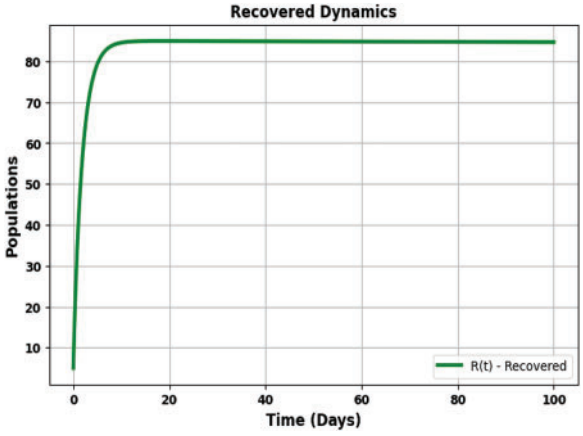

Figure 18: Plot for change in recovery rate

The figures represent the dynamics of various compartments in an epidemic model under varying conditions.

Fig. 19 shows the susceptible population dynamics, where the population initially grows and stabilizes over time, reflecting the influence of external factors affecting susceptibility.

Fig. 20 illustrates the exposed population dynamics. The exposed population rapidly increases before reaching a plateau, indicating a steady state in the progression from exposure.

Fig. 21 presents the infected population dynamics. The infected population rises initially and then stabilizes, representing the equilibrium reached due to infection spread and recovery.

Fig. 22 demonstrates the quarantined population dynamics. The quarantined population exhibits a similar trend, quickly reaching a stable state, which highlights effective containment measures.

Lastly, Fig. 23 captures the recovery dynamics, where the recovered population increases significantly and stabilizes over time, emphasizing the recovery rate's role in the model.

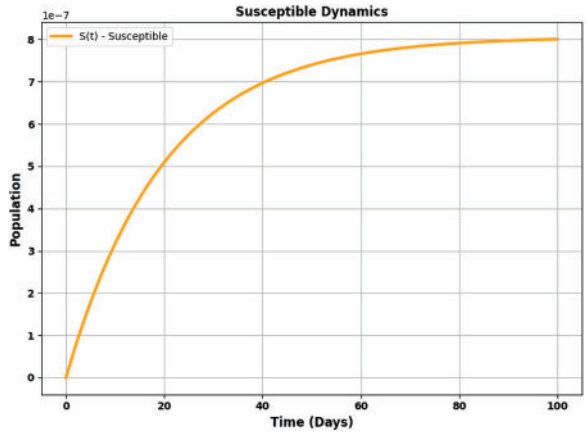

Figure 19: Plot for change in susceptible rate

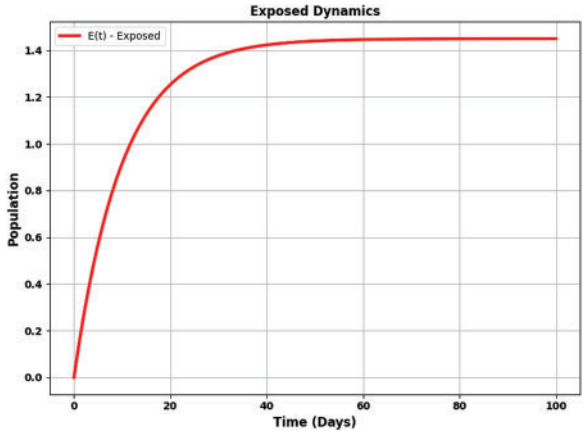

Figure 20: Plot for change in exposed rate

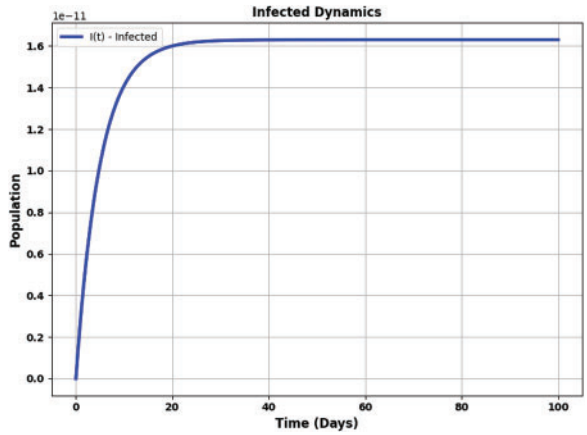

Figure 21: Plot for change in infected rate

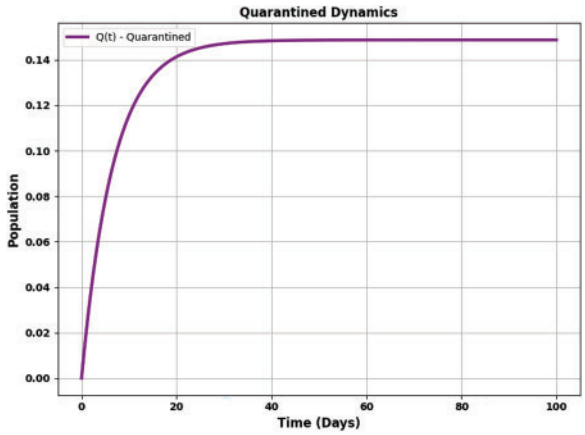

Figure 22: Plot for change in quarantine rate

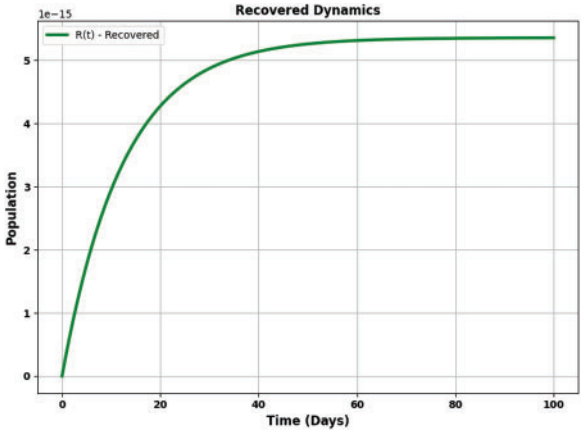

Figure 23: Plot for change in recovery rate

11 Conclusion

This study presents a mathematical model of COVID-19 using the SEIQR system of differential equations, incorporating key parameters such as the susceptible rate (A), contact rate (β), progression rate (ϵ), and recovery rates (α_1, α_2). The model's inclusion of optimal control strategies (v_1, v_2, and v_3) offers a valuable tool for minimizing the epidemic's spread and impact.

Numerical simulations reveal that without intervention, the susceptible population increases sharply, highlighting the potential strain on healthcare systems. However, quarantine and recovery strategies significantly reduce the number of exposed and infected individuals, illustrating the model's responsiveness to public health measures. At day 90, the model demonstrates the effectiveness of isolation and quarantine in controlling the disease, despite a large susceptible population.

The optimal control analysis underscores the importance of balancing intervention strategies. Without intervention, the epidemic's cost is highest, but applying isolation maximally results in the lowest cost, demonstrating its effectiveness in reducing transmission. Quarantining exposed individuals and implementing hygiene measures also show benefits, though they are less impactful alone. A combination of all three strategies proves to be the most effective approach for controlling the epidemic.

This model addresses several key gaps in the existing literature on epidemic modeling. While traditional models have focused primarily on the SEIQR framework, they often overlook the impact of quarantine and hygiene measures. Additionally, many models do not incorporate optimal control theory, which this study uses to assess the cost-effectiveness of various intervention strategies. By combining these elements, the model provides a more realistic and actionable framework for epidemic management, offering practical insights into how policymakers can effectively allocate resources and design interventions.

The integration of optimal control theory with the SEIQR framework is a significant novelty of this model. While many existing models explore disease dynamics, few examine the synergistic effects of multiple intervention strategies like isolation, quarantine, and hygiene measures. This holistic approach, combined with real-time validation using data from Tamil Nadu, India, offers a more detailed understanding of epidemic control. It provides a dynamic tool for evaluating the effectiveness

of public health strategies, making it highly relevant for managing both the public health and economic impacts of future epidemics.

In conclusion, this study fills a critical gap in epidemic modeling by offering a novel approach that integrates optimal control with disease dynamics. The model's ability to assess the cost-effectiveness of interventions and its real-world applicability make it a valuable resource for guiding public health policies and strategies in future epidemic scenarios. The current model can be extended by adopting stochastic processes, incorporating time delay, and analyzing fractional order versions. The above-discussed concepts represent the new gateway for future research.

Acknowledgement: The researchers would like to thank the Deanship of Graduate Studies and Scientific Research at Qassim University for financial support (QU-APC-2025).

Funding Statement: This study was supported by the Deanship of Graduate Studies and Scientific Research at Qassim University (QU-APC-2025).

Author Contributions: Ramesh Ramalingam: Writing—review & editing, Writing—original draft, Project administration, Methodology, Investigation, Formal analysis, Conceptualization. **Arul Joseph Gnanaprakasam:** Writing—review & editing, Writing—original draft, Validation, Supervision, Methodology, Investigation. **Salah Boulaaras:** Writing—review & editing, Writing—original draft, Validation, Supervision, Methodology, Investigation. All authors reviewed the results and approved the final version of the manuscript.

Availability of Data and Materials: The data that support the findings of this study are available from the authors, Ramesh Ramalingam, Arul Joseph Gnanaprakasam, and Salah Boulaaras, upon reasonable request.

Ethics Approval: Not applicable.

Conflicts of interest: The authors declare no conflicts of interest to report regarding the present study.

References

1. Bernoulli D. (1760) Essai d'une nouvelle analyse de la mortalité causée par la petite vérole et des avantages de l'inoculation pour la préevenir. In Màemoires de Mathéematiques et de Physique. Paris: Acadàemie Royale Des Sciences; 1760. p. 1–45.
2. Kermack WO, McKendrick AG. Contributions to the mathematical theory of epidemics-I. Proc R Soc A. 1927;115(772):700–21. doi:10.1098/rspa.1927.0118.
3. Krener AJ. The high order maximal principle and its application to singular extremals. SIAM J Control Optim. 1977;15(2):256–93. doi:10.1137/0315019.
4. Guckenheimer J, Holmes P. Nonlinear oscillations, dynamical systems, and bifurcations of vector fields. New York: Springer-Verlag; 1983. doi:10.1007/978-1-4612-1140-2.
5. Diekmann O, Heesterbeek JAP, Metz JAJ. On the definition and the computation of the basic reproduction number R0 in models for infectious diseases in heterogeneous populations. J Math Biol. 1990;28(4):365–82. doi:10.1007/BF00178324.
6. World Health Organization. Coronavirus disease 2019 (COVID-19) situation report; 2020.
7. World Health Organization. WHO Director-General's opening remarks at the media briefing on COVID-19; 2020. [cited 2025 Mar 10]. Available from: https://www.who.int/director-general/speeches/detail/who-director-general-s-opening-remarks-at-the-media-briefingon-covid-19,11-03-2020.

8. Johns Hopkins University. COVID-19 dashboard by the center for systems science and engineering (CSSE); 2023. [cited 2025 Mar 10]. Available from: https://coronavirus.jhu.edu/map.html.
9. Centers for Disease Control and Prevention. How COVID-19 Spreads. 2020. [cited 2025 Mar 10]. Available from: https://www.cdc.gov/coronavirus/2019-ncov/prevent-getting-sick/how-covid-spreads.html.
10. Andersen KG, Rambaut A, Lipkin WI, Holmes EC, Garry RF. The proximal origin of SARS-CoV-2. Nat Medi. 2020;26(4):450–2. doi:10.1038/s41591-020-0820-9.
11. Van Doremalen N, Bushmaker T, Morris DH, Holbrook M, Gamble A, Williamson BN, et al. Aerosol and surface stability of SARS-CoV-2 as compared with SARS-CoV-1. N Engl J Med. 2020;382(16):1564–7. doi:10.1056/NEJMc2004973.
12. Mayo Clinic. COVID-19 (coronavirus): symptoms and causes; 2020. [cited 2025 Mar 10]. Available from: https://www.mayoclinic.org/diseases-conditions/coronavirus/symptoms-causes/syc-20479963.
13. International Monetary Fund. World economic outlook, April 2020: the great lockdown; 2020. [cited 2025 Mar 10]. Available from: https://www.imf.org/en/Publications/WEO/Issues/2020/04/14/weo-april-2020.
14. Ministry of Health and Family Welfare, Government of India. COVID-19 dashboard. 2022. [cited 2025 Mar 10]. Available from: https://www.mohfw.gov.in/.
15. The Lancet. India's COVID-19 emergency. India's COVID-19 emergency. The Lancet. 2021;397(10286):1683. doi:10.1016/S0140-6736(21)01052-7.
16. Ferguson NM, Laydon D, Nedjati-Gilani G, Imai N, Ainslie K, Baguelin M, et al. Impact of non-pharmaceutical interventions (NPIs) to reduce COVID-19 mortality. Imperial College London Report; 2020. doi:10.25561/77482.
17. Lenhart S, Workman JT. Optimal control applied to biological models. Boca Raton: CRC Press; 2007. doi:10.1201/9781420011418
18. Buonomo B, d'Onofrio A, Lacitignola D. Global stability of an SIR epidemic model with information-dependent vaccination. Math Biosci. 2008;216(1):9–16. doi:10.1016/j.mbs.2008.08.002.
19. Li L, Wang CH, Wang SH, Li MT, Yakob L, Cazelles B, et al. Hemographic fever with renal syndrome in China: mechanism on two distinct annual peaks and control. Int J Biomath. 2018;11(2). doi:10.1142/S1793524518500308.
20. Kar TK, Nandi SK, Jana S, Mandal M. Stability and bifurcation analysis of an epidemic model with the effect of media. Chaos Solitons Fractals. 2019;120:188–99. doi:10.1016/j.chaos.2019.01.037.
21. Li Q, Guan X, Wu P, Wang X, Zhou L, Tong Y, et al. Early transmission dynamics in Wuhan, China, of novel coronavirus-infected pneumonia. N Engl J Med. 2020;382(13):1199–1207. doi:10.1056/NEJMoa2001316.
22. Guan WJ, Ni ZY, Hu Y, Liang WH, Ou CQ, He JX, et al. Clinical characteristics of coronavirus disease 2019 in China. N Engl J Med. 2020;382(18):1708–20. doi:10.1056/NEJMoa2002032.
23. Berhe HW, Gebremeskel AA, Melese ZT, Al-arydah M, Gebremichael AA. Modeling and global stability analysis of COVID-19 dynamics with optimal control and cost-effectiveness analysis. Partial Differ Equ Appl Math. 2024;11(1–2):100843. doi:10.1016/j.padiff.2024.100843.
24. Prem K, Liu Y, Russell TW, Kucharski AJ, Eggo RM, Davies N. The effect of control strategies to reduce social mixing on outcomes of the COVID-19 epidemic in Wuhan, China: a modelling study. Lancet Public Health. 2020;5(5):e261–e270. doi:10.1016/S2468-2667(20)30073-6.
25. Bhuyan A. COVID-19: india's health system faces the aftermath of a second wave. Lancet. 2021;397(10281):1873. doi:10.1016/S0140-6736(21)01116-9.
26. Dutta B. COVID-19 vaccination drive in India: progress and challenges. Indian J Med Res. 2021;153(5):599–601. doi:10.4103/ijmr.IJMR-2131-21.
27. Nicola M, Alsafi Z, Sohrabi C, Kerwan A, Al-Jabir A, Iosifidis C, et al. The socio-economic implications of the coronavirus pandemic (COVID-19): a review. Int J Surg. 2020;78(3):185–93. doi:10.1016/j.ijsu.2020.04.018.

28. Samui P, Mondal J, Chatterjee AN, Al Basir F. Impact of awareness in self-monitoring of COVID-19: an optimal control approach. Results Control Optim. 2025;18:100513. doi:10.1016/j.rico.2024.100513.
29. Ramesh R, Arul Joseph G. SEIHR model for Indian COVID-19: trustworthiness of the government regulatory procedure for coronavirus aspects. Commun Math Biol Neurosci. 2024;2024:24. doi:10.28919/cmbn/8407.
30. Ramesh R, Arul Joseph G. The optimal control methods for the Covid-19 pandemic model's precise and practical SIQR mathematical model. IAENG Int J Appl Math. 2024;54(8):1657–72.
31. Samui P, Mondal J, Ahmad B, Chatterjee AN. Clinical effects of 2-DG drug restraining SARS-CoV-2 infection: a fractional order optimal control study. J Biol Phys. 2022;48(4):415–38. doi:10.1007/s10867-022-09617-9.
32. Liu Y, Ning Z, Chen Y, Guo M, Liu Y, Gali NK, et al. Aerodynamic analysis of SARS-CoV-2 in two Wuhan hospitals. Nat. 2020;582(7813):557–60. doi:10.1038/s41586-020-2271-3.
33. Madubueze CE, Dachollom S, Onwubuya IO. Controlling the spread of COVID-19: optimal control analysis. Comput Math Methods Med. 2020;2020(1):6862516–14. doi:10.1155/2020/6862516.
34. GAVI. India's COVID-19 second wave: the race to vaccinate. Global Alliance for Vaccines and Immunizations (GAVI); 2021. [cited 2025 Mar 10]. Available from: https://www.gavi.org/vaccineswork/indias-covid-19-second-wave-race-vaccinate.
35. Kaggle. Epidemic model: cOVID-19 India visualizations. [cited 2025 Mar 10]. Available from: https://www.kaggle.com/code/chekoduadarsh/epidemic-model-covid-19-india-visualizations/input.